IMPROVING THE UNDERSTANDING OF ENVIRONMENTAL STRESS CRACKING IN POLYETHYLENES

IMPROVING THE UNDERSTANDING OF ENVIRONMENTAL STRESS CRACKING IN POLYETHYLENES BY MODIFICATION OF THE BELL TEST

BY

VLADIMIR GRITSICHINE, B. ENG.

A Thesis

Submitted to the School of Graduate Studies in Partial Fulfillment of the Requirements for the Degree of Master of Applied Science

McMaster University

MASTER OF APPLIED SCIENCE (2022) McMaster University

(Chemical Engineering) Hamilton, Ontario

TITLE: Improving the Understanding of Environmental Stress Cracking of Polyethylene

AUTHOR: Vladimir Gritsichine

B.Eng. (Chemical Engineering, McMaster University)

SUPERVISORS: Professor Dr. Michael R. Thompson

Professor Emeritus Dr. John Vlachopoulos

NUMBER OF PAGES: XVI, 124

Lay Abstract

Plastic products and liquid chemicals interact every day, for example, shampoo bottles, gasoline jerrycans, and piping for water or oil. However, with many different polymer–chemical interactions possible, inconsistent and irregular behaviours can cause these polymers to fail prematurely. The project described in this thesis examined modifications to the most commonly used accelerated testing standard for estimating the lifetime of polyethylenes when in contact with chemicals. The first main study of this work considered changes to specimen preparation for the test, using a heat blade to produce more consistent failure times among repeats. The second main study examined the use of a colorimetric tracking dye and computer vision analysis system to monitor aspect of plastics while environmental cracking started and propagated, so that more could be learned about this important failure mechanism.

Abstract

One of the most common failures of plastics while in use is environmental stress cracking (ESC). Studies were conducted in this thesis to improve our understanding of ESC, through experimentation to modify the existing and most-used standardized test for ESC, namely the Bell Test (ASTM D-1693). Given the large variability of failure times associated with the Bell Test, the first study consisted of developing a novel heat notching technique. This technique consisted of a heated blade used for notching and showed decreased variability compared to the standard method of notching. Given the success, this work further highlighted a growing theory that the local phase morphology of the notch was critically important to assessing environmental stress cracking resistance.

The second study in this thesis explored the ESC failure mechanism on this new viewpoint that the local region of the notch and the structural arrangement of polyethylene therein was critically influential. The work related the failure mechanism to the localized absorption of the typical stress cracking agent, IGEPAL CO-630, in conjunction with the localized stress development in the notch, using an organic dye tracer and computer vision aided analysis. The study reinforced the importance of the local amorphous and crystalline regions, seen in the heat notch study, and found a two-stage stress-dependent absorption mechanism for IGEPAL occurring as cracking developed in the polyethylene samples.

Acknowledgements

It has been a long yet fruitful endeavor completing this work. However, I am not the sole reason for the success of this work as it couldn't have been done without the help, guidance, and motivation from my supervisors, peers, and technical collaborators. Firstly, I would like to thank Imperial Oil Ltd, for providing the funding and opportunity for this work, and Ron Cooke at Imperial Oil for his wonderful advice, technical insights, and supply of materials throughout the duration of this work.

I want to sincerely thank my supervisor, Dr. Michael Thompson, for his unwavering support, trust, patience, and guidance throughout the last three years. Thank you for taking me on as a student in your lab group and providing me with many advantageous opportunities to learn a substantial number of theories and skills I would have never of thought I would be able to learn. I would also like to thank my co-supervisor, Dr. John Vlachopoulos for his technical and helpful insights, as well as his first-class advice during our meetings throughout the years.

I would like to express my gratitude to Heera Marway, who not only collaborated with me on one of my manuscripts but provided me with an altruistic standard of how one should conduct work with others. I have learnt many lessons from you, and I am grateful to have worked with you throughout my time here. I would also like to highlight my colleagues, Austin Bedrosian and Hassan Abdulhussain. Without your endless encouragement, belief, and discussions, this work wouldn't have been half of what it is today. Thank you for standing by my side.

This thesis would not have been possible without the invaluable support, love, encouragement, and backing of my parents, Diana and David. Finally, I would like to thank my partner Laura for being my pillar during the hard times of this work.

Aut viam inveniam aut faciam

Table of Contents

List of Figures

List of Tables

Chapter 1. Introduction

Polyethylene is a semi-crystalline polymer and one of the most used thermoplastics in the world, with a 31.2% share of the thermoplastic market and a global demand of 154 billion pounds yearly [1,2]. In North America, 22% of the global supply of polyethylene is used [1]. The reasons for polyethylene's popularity include its low cost and enhanced processability, as well as favourable properties like chemical resistance, toughness, flexibility at low temperatures, film clarity, and low water permeability, making it well suited to many packaging, piping, and agricultural applications [2,3]. The application of focus for this thesis is buried polyethylene piping for water and gas [4]. This use was initially started by the DuPont Company for transporting natural gas back in 1965 [4].

With the increased usage of polyethylene piping for municipal purposes, it is important to determine how long these pipes will last before leakage, lest significant environmental damage be allowed to occur. The failure mode producing leakage is a process called slow crack growth, where crazing of polyethylene occurs to create a point of stress concentration [4]. This crazing can occur at defects such as scratches, cuts, and notches, which further serves as a point of stress [4]. This point of stress further governs the rate of growth, and over time crazing grows, further leading to crack initiation, then propagation and eventually, the rupture of a pipe [4,5]. However, it has been observed that this process can be accelerated when the polymer part is in contact with gasolines, gases, various chemicals, and even sewage fluid [5]. The accelerated phenomenon is known as environmental stress cracking, which causes rapid and catastrophic failure within

polyethylene without any warning [5]. Environmental stress cracking occurs when certain fluids are absorbed and plasticize the material at hand [6]. This absorption phenomenon further accelerates the crazing as well as crack growth of the material.

Recently engineered polyethylene grades combat environmental stress cracking by focusing on specific structural properties [3,7–10] . Primarily, it has been noted in various literature sources that crystallinity has a variable yet monumental effect on resisting environmental stress cracking [7,11]. Annealing and quenching studies with polyethylene have shown increased variability in the failure times of samples being tested for environmental stress cracking [12,13]. This effect was attributed to how the amorphous and crystalline phases change through the course of heating and cooling polyethylene parts [12,13].

Despite these new grades of resin being now available for use, environmental stress cracking remains a great concern to the infrastructure of oil and water transport, and thus it is important to understand how this phenomenon starts, progresses, and finishes. An important tool for this exploration is the Bell Test, where ten U-bent rectangular specimens are exposed to a stress cracking agent in a controlled environment meant to accelerate the failure. Previous studies revealed that the initial defect of the material is the primary driver of failure for environmental stress cracking and the absorption of the stress cracking fluid is the secondary driver. One recent study found biodiesel as a stress cracking fluid but more importantly, due to its yellow colour, was noted to preferentially diffused into the stress concentrated region of the bent Bell-Test specimen [14]. From this finding, it was

hypothesized that a greater focus should be given to the region of the initial defect in hopes of further understanding environmental stress cracking.

To investigate the initial defect, two studies were undertaken with the goal to explore the phase morphology in the local region of the notch and its effects on failure as well as variability, and the determination of the relation between the failure mechanism and the localized absorption as well as development of stresses in the initial defect.

The first drafted manuscript shown in Chapter Three, shows results from the initial studies conducted with the Bell Test. This study explores a new notching technique consisting of a heated blade. The second drafted manuscript shown in Chapter Four builds upon Chapter Three's main idea of local phase morphology holding great importance when testing for environmental stress cracking. This drafted manuscript set out to relate the failure mechanism of environmental stress cracking to the localized absorption of the stress cracking agent, as well as the development of stresses within the notch. A drafted technical communication relating to the automation of the Bell Test can be seen in Chapter 5. This chapter describes in detail the evolution of a computer vision technique used in Chapter 4, meant to help the industry improve their use of the Bell Test.

References

[1] T.E. Nowlin, Business and Technology of the Global Polyethylene Industry, 2014.

[2] S. Ronca, Polyethylene, Elsevier Ltd, 2017. https://doi.org/10.1016/B978-0-323-35824-8.00010-4.

[3] M. Demirors, The History of Polyethylene, 2011. https://doi.org/10.1007/978-1-4614-6504-1_1.

[4] N. Brown, Intrinsic Life Time of Polyethylene Pipelines, Polymer Engineering and Science. 47 (2007) 477–480. https://doi.org/10.1002/pen.

[5] J.J. Cheng, M.A. Polak, A. Penlidis, Influence of micromolecular structure on environmental stress cracking resistance of high density polyethylene, Tunnelling and Underground Space Technology. 26 (2011) 582–593. https://doi.org/10.1016/j.tust.2011.02.003.

[6] D. Wright, Environmental Stress Cracking of Plastics, 1st ed., Rapra Technology Limited, 1996.

[7] P.D. Frayer, P.P. Tong, W.W. Dreher, The role of intercrystalline links in the environmental stress cracking of high density polyethylene, Polymer Engineering & Science. 17 (1977) 27–31. https://doi.org/10.1002/pen.760170105.

[8] J. Cazenave, B. Sixou, R. Seguela, Structural Approaches of Polyethylene Environmental Stress-Crack Resistance, Oil & Gas Science and Technology. 61 (2006) 735–742. https://doi.org/10.2516/ogst.

[9] M. Razavi-Nouri, J.N. Hay, Thermal and dynamic mechanical properties of metallocene polyethylene, Journal of Applied Polymer Science. 42 (2001) 8621–8627. https://doi.org/10.1002/app.1988.070350710.

[10] L. D'Agnillo, J.B.P. Soares, A. Penlidis, Controlling molecular weight distributions of polyethylene by combining soluble metallocene/MAO catalysts, Journal of Polymer Science, Part A: Polymer Chemistry. 36 (1998) 831–840. https://doi.org/10.1002/(SICI)1099-0518(19980415)36:5<831::AID-POLA16>3.0.CO;2-H.

[11] S. Bandyopadhyay, H.R. Brown, Evidence of interlamellar failure in environmental stress cracking of polyethylene, Journal of Materials Science. 12 (1977) 2131–2134. https://doi.org/10.1007/BF00561990.

[12] X. Lu, N. Brown, Effect of thermal history on the initiation of slow crack growth in linear polyethylene, Polymer (Guildf). 28 (1987) 1505–1511. https://doi.org/10.1016/0032-3861(87)90350-8.

[13] S.R. Ghaffarian, N. Mohammadi, A. Sharif, Model Prediction of the ESCR of Semicrystalline Polyethylene: Effects of Melt Cooling Rate, Journal of Applied Polymer Science. 116 (2008) 2658–2667. https://doi.org/10.1002/app.

[14] A.K. Saad, H.A. Abdulhussain, F.P.C. Gomes, J. Vlachopoulos, M.R. Thompson, Studying the mechanism of biodiesel acting as an environmental stress cracking agent with polyethylenes, Polymer (Guildf). 191 (2020) 122278. https://doi.org/10.1016/j.polymer.2020.122278.

Chapter 2. Literature Review

2.1 Progression of Environmental Stress Cracking Failure

One major shortcoming of polymeric materials is the loss of mechanical properties when exposed to adverse environments. Glassy polymers such as polycarbonate, polysulfone, pol(2,6-dimethyl-1,4 phenylene oxide) (PPO), and PPO/polystyrene blends display immediate failure when experiencing moderate applied stresses and in contact with specific organic liquids [1–5]. In some rare instances, internal stresses within glassy polymers can be a sufficient driver for failure when in contact with organic fluids [4,5]. However, this problem is not limited to just glassy polymers, and extends to semi-crystalline polymers. Semi-crystalline polymers, although much more resistant to various environments, have been documented to fail in applications consisting of various environments [6–12].

Polyethylene, being the primary focus of this thesis, is historically one of the first semi-crystalline polymers to have been recorded to fail due to its environment [5,13]. Relating to the wire and cable industry, low density polyethylene (LDPE) was used as a replacement sheathing for unsaturated cross-linked elastomers [5,13]. Typically, the cross-linked elastomers would be coated with a surfactant to lower its friction when the wire was pulled through a conduit [5,13]. When this practice with the surfactant was first applied to LDPE sheathing there was a rash of failures witnessed related to its presence [5,13]. This failure was more prevalent in wire and cables that were bent, resulting in stress induced failures [5,13]. This finding led to a testing method and a new failure mechanism for

polymers, environmental stress cracking. Environmental stress cracking (ESC) has been defined as the acceleration of stress cracking by contact with a fluid [6,14–16]. ESC is a purely physical mechanism (i.e. no chemical reaction) and is based on interactions between a polymer and fluid [6,14–19]. Typically, the fluid accelerating ESC is labelled as a stress cracking agent, which when adsorbed, absorbed, and plasticizing the polymer containing stresses, causes eventual failure [6,14–19]. Stress cracking agents come in a broad range of fluids, including but not limited to, soaps, wetting agents, oils, and detergents [6,14–19].

To understand the ESC mechanism, a pre-requisite of slow crack growth knowledge is needed. The primary difference between the two, is that slow crack growth doesn't require an aggressive environment for failure [1,7,14,20]. Both failures contain similar macroscopic mechanisms of failure, where craze initiation, craze growth, crack initiation, crack propagation, and residual fracturing occur [6,7,15–17,21]. When a specimen is faced with a load either below yielding or above, it is theorized that a craze at the root of the initial defect occurs [21]. The size of the craze can be predicted by the Dugdale theory, which is inversely proportional to the yielding point [21]. Once the craze is established, a relaxation of stresses occurs causing the craze to increase in size [21,22]. Crack initiation originates from the increasing local stresses associated with craze growth within the notches, defects, and other imperfections placed within the material [6,14,15]. After a crack is initiated at a microscopic scale, a craze-crack growth mechanism starts, where micro-voids form perpendicular to the local defect [15,23,24]. Over time these voids grow larger, causing fibrils from the crystalline region to appear, known as crazing [14,15,17,25]. Residual fracture happens when the fibrils break apart within the crazing zone, causing the

crack to be visible. The difference between slow crack growth and environmental stress cracking is that craze initiation and craze growth is accelerated by the diffusion of the stress cracking agent in the latter case [1,7,14,20]. Thus, slow crack growth is an intrinsic property of the polymer, and environmental stress cracking is an extrinsic property due to the acceleration of the stress cracking agent. To further understand environmental stress cracking with regards to what happens to polyethylene throughout the process, knowledge of the various microstructures of polyethylene followed.

Considering polyethylene is a semi-crystalline polymer, there are amorphous and crystalline phases present. Crystalline regions contain lamellae, which are connected by tie molecules to make up the definite structure of the polyethylene. These tie molecules may span across various amorphous regions to make connections with lamellae [20,26]. Additionally, there are two types of tie molecules. The first being bridging tie molecules, formerly described as two ends of the molecule being crystallized in two separate lamellae [20]. The second type of tie molecule consists of inter-lamellar linkages, which are entanglements supported by Van der Waals forces [20]. Amorphous contents consist of molecular entanglements containing molecules and chains which are shorter in size [20,27]. Chains and molecules which don't end up becoming bridging tie molecules typically combine to form entanglements within the amorphous regions of polyethylene [20,27]. The entanglements within the amorphous regions surrounding the crystalline regions can be further categorized as loose loops (which are chains having both ends of the molecule in the same lamella) or cilia (which contain one end of the molecule connected to a lamella, while the other end being untethered) [27].

In the face of a load in the normal direction, the crystalline regions slip past one another, causing a strain on the tie molecules present [7,20,21,26,27]. Over time, these tie molecules cannot hold the crystalline regions together and fail. This dislocation degrades the lamellas and spherulites present in the polyethylene, seen as crazing [28–31]. Over time the applied normal load to the polyethylene and the degradation of crystalline content leads to an increased rate of disentanglements of tie molecules, thus leading to the relaxation of stresses present in the polyethylene [14,20]. This leaves behind the growth of micro-voids, not apparent to the eye, and further facilitates the craze-crack growth mechanism [15]. The above mechanism is how slow-crack growth is facilitated throughout the microstructure of polyethylene, namely by craze initiation, craze growth, and crack initiation.

Although environmental stress cracking is considered a modified failure mechanism of slow crack growth, it is further important to know how the stress cracking fluid interacts with polyethylene to lead to an accelerated failure. Early studies indicated that the stress cracking agents and its contact surface allow for a reduction of surface energies allowing a lower required amount of energy for craze formation to crack initiation [5]. However, the reduction of surface energy for craze formation is now considered a minor effect to the overall ESC mechanism [5]. It has been reported in glassy polymers that the stress cracking agents acts as a plasticizer, creating larger internal stresses due to increasing osmotic pressures from the subsequent diffusion of the agent [5,32]. However, the later part of the mechanism is generally discredited in current ESC research, as stress cracking agents show limited bulk adsorption throughout the specimen [5]. The whole

mechanism is still evident in the swelling of non-solvent exposed glassy polymers which are not apart of this study.

Recent literature incorporates both ideas mentioned above, where the stress cracking agent diffuses into the polymer at hand, primarily in the amorphous region, providing plasticization-like effects that further accelerates the slow crack growth mechanism during the craze initiation, craze growth, and crack initiation [7,15,19,21]. This is further confirmed through recent studies where the stress cracking agent was found to locally diffuse into the amorphous regions of a defect in a polyethylene part while under normal load, causing stress induced swelling as well as the aforementioned plasticization-like effect [14,19]. However, it has been argued that some amount of diffusion of the stress cracking agent occurs into the highly deformed crystalline regions as well, making them weaker over time [21,25]; though this is not considered the dominant path of absorption within polyethylene. Once absorbed into the amorphous regions, the swelling of the amorphous regions along with the normal force applied to the polyethylene, causing accelerated slippage and breakage of crystalline contents [15,21,25,33]. The tie molecules holding together various lamellas further disentangle at an increased rate observed in slow crack growth, further causing craze growth as well as crack initiation to occur [21,25]. Depending on the severity of the fluid in contact with the polyethylene, crack propagation can be accelerated.

The stress cracking agent-polyethylene boundary depends on the stress cracking agent's properties. Kambour et al, measured a range of solubility parameters (δ) of various plastics and organic fluids, and determined that the minimum value of critical strain to

cause crazing happened at $\delta_{liquid} = \delta_{plastic}$ [5,15,34]. This was found by plotting various critical strains along the solubility parameters determined. It was thought that the differences between both solubility parameters (i.e. total cohesive attraction between fluid molecules) can be seen as the plasticization efficiency [15]. Consequentially, plasticization-like effects are expected when solubility parameters are close together in value; the plastic as well as the liquid can become miscible between molecular interactions [34]. Furthermore, if the solubility parameters are far apart from each other, embrittlement of polyethylene occurs [6]. An excellent example of solubility parameters being like each other is IGEPAL CO-630, a nonylpheoxy poly(ethyleneoxy) ethanol and polyethylene, respectively having values of 20.0 $MPa^{1/2}$ and 16.4 $MPa^{1/2}$ [6,15]. This fluid combination is a standard for testing and is the primary focus of the work highlighted in the next sections.

Given the importance of the solubility parameters, Tonyali et al. proposed a mechanism which provided an explanation of how IGEPAL CO-630 interacts with polyethylene. It is proposed that since IGEPAL CO-630 is a commercial detergent, containing impurities such as nonylphenol and polyethylene glycol (1%), these impurities may cause the acceleration of cracking [15]. It is suggested that due to the solubility parameter of nonyl phenol (19.4 $MPa^{1/2}$), that nonylphenol is easily soluble with IGEPAL CO-630 and not water, thus allowing nonylphenol to be bound within IGEPAL CO-630 micelle in water and attracting these micelles to the surface of polyethylene [15]. Due to this phenomenon, the described stress induced swelling as well as plasticization-like effects mentioned previously can happen. It is noted that different fluids contain different methods of conveying the fluids to the surface of the plastic, however the primary focus of this work

is an environment consisting of polyethylene and IGEPAL CO-630 and hence it is discussed. With an infinite number of plastic-fluid combinations available, Wright proposed six general predictors constituting to ESC occurring between plastic and fluids. This is summarized below [6].

1. Amorphous thermoplastics and glassy polymers in an amorphous state are more prone to ESC than semi-crystalline polymers.
2. Fluids containing modest hydrogen bonding are more likely to be severe or moderate stress cracking agents
3. Fluids with high molecular weights are not likely to be severe stress cracking agents
4. Fluids near their boiling temperature increasingly provide an aggressive environment for ESC to be carried out in.
5. Glassy polymers are more prone to ESC at temperatures near their glass transition temperature.
6. Low molecular weight polymers are more likely to face ESC

With an understanding of craze initiation, craze growth, and crack initiation, the next steps in understanding the environmental stress cracking mechanism are how crack propagation and residual failure happens. A four step cracking propagation mechanism was proposed by Tonyali et al. , and was used as the basis in current literature relating to biodiesel as a stress cracking agent when in contact with polyethylene [19]. This mechanism serves as the basis of understanding on how crack propagation progresses throughout the thesis' works presented in later sections and can be seen below [15].

1. Fibrillar fracture happens at the crack tip of samples facing a normal load (i.e bent specimens)
2. The environment consisting of IGEPAL CO-630, nonylphenol, and water wets the fibrils without any restriction, leading to micelles being absorbed into the fibrils.
3. Diffusion of aggressive molecules occurs at areas where stress is the highest, prevalent with microstructures that are unoriented, as they are reported to fail first. Typically, this occurs at the stems of the fibrils. Following the failure of unoriented microstructures, structures containing efficient chain packing subsequently fail after.
4. The stress-diffused molecules in the stressed polyethylene further plasticizes the material, increasing fibril breakdown at an increased rate, leading to crack growth.

With the mechanism of crack propagation and the interactions between a crack-initiated surface and a stress cracking agent leading up to this moment highlighted above, various factors such as the characteristics of crystallinity and amorphous contents affect the progression of ESC failure. These characteristics can be modified throughout the development of various polyethylene grades, as well as post treatment of polyethylene described in the next section.

2.2 Processing Factors Influencing Environmental Stress Cracking within Polyethylene

There are a lot of factors which influence environmental stress cracking within polyethylenes but most influential is the arrangement and distribution of amorphous and crystalline phases. It is important to look at how polyethylene is made, as depending on the additives as well as catalysts used, the molecular weight distribution as well as distribution of amorphous and crystalline phases will heavily impact environmental stress cracking resistance (ESCR). Typically, the monomer, comonomers, chain-transfer agents, catalysts and solvents are fed into either continuous stirred tank reactors or loop reactors where the temperature of the reactor remains below the polymer's melting point [35–37]. Once all the items are fed into the reactor, a series of reactions including the crystallization of ethylene monomers, occurs in the reactor [35]. These reactions result in a slurry of solid particles within the solvent media [35]. Solid polyethylene particles are further separated from the solvent, mixed, pelletized, and packaged for the consumer [35]. When various comonomers and catalysts are used within the described reaction above, its molecular properties such as branching nature become altered, further affected ESCR behaviour [35–37].

The two primary polyethylene grades of concern throughout the studies conducted in this thesis were high density polyethylene, and linear low-density polyethylene. When high molecular weight high density polyethylene is slowly cooled, studies revealed that a higher amount of stress cracking agent is absorbed when compared to a quenched sample [28,31]. This was determined by their percent change in toughness, where the stress cracking agent held higher plasticization effects then samples which were quenched or

unaltered [31]. Ultimately, with an increased absorption of the stress cracking fluid, ESCR is seen to decrease. This is due to the slowly cooled polyethylene having higher permeability and thus increased capacity to absorb the stress cracking fluid [31]. Further, when the high molecular weight high density polyethylene was quenched during heat treatments, it was found that the yield point was higher and consequentially, quenching lowered the absorption of stress cracking agents [31]. Similar studies undertaken with low molecular weight linear low density polyethylene showed that quenching caused under-developed spherulites whereas slowly cooled samples allowed for spherulites to merge closer together [28]. In addition, quenching further halts the development of spherulites to merge or form, causing the increased packing of smaller and underdeveloped spherulites. The increased presence of these underdeveloped spherulites being in proximity of each other allowed for smaller and finer spaces to occur between spherulites. In comparison, fully developed spherulites, although larger in size, contain increased gaps between spherulites. The underdeveloped spherulites were further shown to impede the absorption of the stress cracking agent, through a reduction of available pathways for absorption to occur. These underdeveloped spherulites further act as a "plug" to solvent ingress and hinder ESC progression. In addition to the increase in spherulites, there is an increased probability of tie molecules, as well as incomplete tie molecules [28]; both cases of these chains which transmit stresses between crystals will delay ESC failure.

The above observations for both low molecular weight linear low density polyethylene and high molecular weight high density polyethylene are not seen for low molecular weight high density polyethylene. Particularly, the two prior polyethylene types

have seen quenching to increase ESCR. However, in a previous study conducted on quenching low molecular weight high density polyethylene, the authors found ESCR worsened [38]. This discrepancy was due to lower molecular weight species having disproportionately more chains between entanglements. Quenching further decreases the number of entanglements, as entanglements combine to form crystalline contents. Conversely, lower molecular weight polyethylenes contain increased amorphous regions with less entanglements as well as tie molecules then polyethylene's with higher molecular weight, resulting in an accelerated opportunity for stress cracking agent to diffuse into the amorphous areas [20,27]. To circumvent the increased rate of failure for low molecular weight high density polyethylene's, annealing or slow cooling after processing allows for an improvement in crystallinity, further improving ESCR [39].

It is seen through heat treatments such as quenching or annealing, that ESCR can be easily affected but not always in a predictable manner. Throughout the literature it is noted that the thermal processing history of polyethylene variably affects ESCR[23] .Tie molecules in conjunction with the affects of entanglements cannot fully describe ESC failure. Since ESC is too complicated to predict, it is important to tests for the ESCR ratings of polymers.

2.3 Testing of Environmental Stress Cracking

There are a variety of tests for the determination of ESCR which serve as predictors to how materials will react under ESC conditions. Primarily, the testing of ESC serves as a ranking as well as a guideline for materials to be used for part designs, quality control of

polyethylene production, as well as research and development. The most popular method of testing is the Bell Test (ASTM D1693), principally used for polyethylenes. This test consists of 10 polyethylene specimens of 38 x 13 x 3 (thickness) mm samples having 18.9 mm long and 0.625 mm deep notches down their middle at the site of bending [40]. The specimens are immersed in either pure IGEPAL CO-630, or a 10% IGEPAL CO-630 solution, kept at 50°C or 100°C (only for the pure IGEPAL CO-630 case) [40]. The measure of ESCR is the time it takes for the five out of the ten samples to fail. This is denoted as the f_{50} metric. Conversely, another method for ESCR takes the percentage of failures on the x axis, and the time of failure on the y axis [40]. However, it is noted that the percentage of failures cannot be 0% or 100% as failures cannot be assumed to always fail or not fail when tested [40]. Linear regression is further performed on the graph, and 50% is used in the acquired line function, producing the F_{50} value [40]. Although the test is simple to implement, it faces various weaknesses in determining this time, such as the operator only needing to check on the status of the test every 12 hours, part failure is a rather subjective observation, and long failure times dependent on the polyethylene grade tested [40]. The delay in failure is typically due to the stress relaxation around the bending stress applied [41]. This type of test is typically known as constant strain test and is the focus of this thesis [41].

The second group of testing methods is based on constant stress. Examples of these methods are the Pennsylvania Notch Test (ASTM F1473) or the Full Notch Creep Test. Both are used to determine slow crack growth resistance of polyethylene pipe materials; however, only the Full Notch Creep Test can be immersed in aggressive stress cracking

agents at elevated temperatures [41,42]. Additionally, the Full Notch Creep Test provides for more flexibility for media as well as the temperature used, whereas the Pennsylvania Notch Test requires a nominal stress of 2.4 MPa, fixed temperature of 80°C, and exposure to air [41,43]. The primary difference in these two tests specimens is that the Full Notch Creep Test contains four coplanar notches in the specimens, while the Pennsylvania Notch Test contains one main notch and two additional notches on the side of the sample [41]. Considering the increased stress concentrations on the samples, the test measures either slow crack growth resistance (Pennsylvania Notch Test), or environmental stress cracking directly (Full Notch Creep Test) [41].

One newer method of determining the environmental stress cracking resistance of polyethylene's is the strain hardening modulus method [41,44–46]. It is noted that one of the primary drivers of ESC is the disentanglement of interlamellar linkages such as the two types of tie molecules and amorphous entanglements [44]. These two factors are critical for strain hardening within polyethylene, thus have been correlated to predict ESC. As a result of this correlation, the strain hardening modulus provided for a convenient and reliable method of ranking ESCR of polyethylene materials using simple tensile tests. One downside of this method is that it only is tested in ambient air [41]. The strain hardening modulus method has been compared to the Notch Constant Load Test, used for polyolefin geomembranes [41,47]. The notch constant load test uses a notched dumbbell shaped sample submerged into a 10% IGEPAL CO-630 solution at 50°C [47]. The applied stress levels throughout testing ranged from 20% to 60% with increasing increments equal to 5% [47]. This test is similar to the Bell Test with the improvement of potentially removing

stress relaxation from bending force, however like all tests mentioned besides the Bell Test, only one specimen is tested at a time [47]. Thus, repeats of tests are time consuming to complete.

Considering the Bell Test is the most convenient type of ESCR test, various improvements can be made to increase the repeatability as well as how failures are detected. With recent advance in technology, exploring how to continuously monitor a Bell Test should yield improvement.

2.4 Neural Networks

With recent advancements in technology, the automation, detection, and inclusion of extra data is thought to improve current ESCR testing. One advancement explored in this thesis is neural networks used to automate and improve current ESCR testing. Neural networks are data processing systems consisting of many simple and interconnected processing elements inspired by the structure of the cerebral cortex portion of the brain [48] . These processing elements in a neural network consist of sequences of layers with full as well as random connections between sequences [49]. The first layer being the input layer is where data is presented to the neural network. Intermediate hidden layers which assign weights and biases to the input determine predictions, while the output layer which allows for tuning of the number of responses of predictions required from the hidden layer [49]. To iterate on hidden layers; hidden layers perform nonlinear transformations by applying the output of weights and biases to the input and passing it along to an activation function [49]. Further these activation functions are chosen by the user when producing a neural

network [49]. The goal of a neural network is to determine the ideal weights and biases within the hidden layers to provide for accurate predictions[49]. This is done through a training process, which is based on a user set of iterations (commonly known as epochs), whereby the model determines an ideal set of weights and biases to provide for its predictions [49]. The training process consists of a user defined cost or loss function being optimized to produce accurate as well as reliable predictions. Throughout training, the weights and biases are continuously updated using an optimizer which is user defined. A typical training cycle for the first epoch can be seen below.

1. Weights and biases are randomly initialized; cannot be set to 0
2. Input layer takes data and feeds it to the hidden layer
3. Hidden layer multiplies the weights to the data and adds biases
4. Output of the hidden layers is fed through an activation function
5. The output of the activation function is then considered as an output (Forward Propagation)
6. Use the output layer (predictions) to compute the cost function for the current iteration
7. The output layer produces predictions, which the true value is subtracted from. This is referred to as the error of the output layer. The previous weights and added biases are transposed onto the newfound error term, and element wise multiplication is conducted upon the derivative of the weights multiplied by the inputs of the previous layer. This process goes back until the input layer. This step

formally computes the partial derivatives needed for the optimizer (Backpropagation Algorithm).

8. Using the newly computed partial derivatives, the cost function can be optimized to determine a new minimum, resulting in updated weights and biases.
9. Once the weights and biases are updated, the second epoch begins at step 2 above

Neural networks can complete objectives that humans and animals are capable of, while a conventional computer model does poorly [48]. Neural Networks are used in a variety of applications, however for the work outlined here, convolutional neural networks were used for object detection, classification, and regression of photos relating to the Bell Test. Convolutional neural networks, like the neural networks explained prior consist of input layers, hidden layers, and output layers. However, convolutional neural networks can transform, downsize, and filter image data in between hidden layers [50,51]. Filtering as well as downsizing image data is typically done by taking a kernel which is a user defined size of pixels and applying it to the photo [50,51]. Further, the kernel can take the darkest or lightest pixel value within photo, and replace all the values within the kernel, causing a new filtered image [50,51]. Conversely, the darkest/lightest pixel can be used to replace the entirety of the kernel, thus downsizing the image [50,51]. Further transformations such as rotating, flipping, and skewing images are simply done by multiplying a set of matrix values to the entirety of the photo, resulting in the image data to be altered when passing through the convolutional neural network [50,51].

References

[1] L.F. Henry, Prediction and evaluation of the susceptibilities of glassy thermoplastics to environmental stress cracking, Polymer Engineering & Science. 14 (1974) 167–176. https://doi.org/10.1002/pen.760140304.

[2] Y.W. Mai, Environmental stress cracking of glassy polymers and solubility parameters, Journal of Materials Science. 21 (1986) 904–916. https://doi.org/10.1007/BF01117371.

[3] L.F. Al-Saidi, K. Mortensen, K. Almdal, Environmental stress cracking resistance. Behaviour of polycarbonate in different chemicals by determination of the time-dependence of stress at constant strains, Polymer Degradation and Stability. 82 (2003) 451–461. https://doi.org/10.1016/S0141-3910(03)00199-X.

[4] L.M. Robeson, Applications of polymer blends: Emphasis on recent advances, Polymer Engineering & Science. 24 (1984) 587–597. https://doi.org/10.1002/pen.760240810.

[5] L.M. Robeson, Environmental Stress Cracking: A Review, Polymer Engineering & Science. 53 (2013) 453–467. https://doi.org/10.1002/pen.

[6] D. Wright, Environmental Stress Cracking of Plastics, 1st ed., Rapra Technology Limited, 1996.

[7] H.R. Brown, A theory of the environmental stress cracking of polyethylene, Polymer (Guildf). 19 (1978) 1186–1188. https://doi.org/10.1016/0032-3861(78)90069-1.

[8] A. Ghanbari-Siahkali, P. Kingshott, D.W. Breiby, L. Arleth, C.K. Kjellander, K. Almdal, Investigating the role of anionic surfactant and polymer morphology on the environmental stress cracking (ESC) of high-density polyethylene, Polymer Degradation and Stability. 89 (2005) 442–453. https://doi.org/10.1016/j.polymdegradstab.2005.01.023.

[9] T. Dooher, A. Saifullah, J. Ullah, C. Magee, A. Mulholland, D. Dixon, Environmental stress cracking of polymers: case studies from industry (ABS and LDPE), Engineering Failure Analysis. (2022) 106120. https://doi.org/10.1016/j.engfailanal.2022.106120.

[10] M.N. Cardoso, A.G. Fisch, Bimodal High-Density Polyethylene: Influence of the Stereoregularity of the Copolymer Fraction on the Environmental Stress Crack Resistance, Industrial and Engineering Chemistry Research. 55 (2016) 6405–6412. https://doi.org/10.1021/acs.iecr.6b00927.

[11] J.W. Wee, Y. Zhao, B.H. Choi, Observation and modeling of environmental stress cracking behaviors of high crystalline polypropylene due to scent oils, Polymer Testing. 48 (2015) 206–214. https://doi.org/10.1016/j.polymertesting.2015.10.011.

[12] B. Tekkanat, B.L. MckKnney, D. Behm, Environmnetal Stress Cracking Resistance of Blow Molded Poly(Ethylene Terephthalate) Containers, Polymer Engineering & Science. 32 (1992) 393–399.

[13] J.B. DeCoste, F.S. Malm, V.T. Wallder, Cracking of Stressed Polyethylene, Industrial & Engineering Chemistry. 43 (1951) 117–121. https://doi.org/10.1021/ie50493a035.

[14] M. Schilling, Environmental Stress Cracking (ESC) and Slow Crack Growth (SCG) of PE-HD induced by external fluids, (2019).

[15] K. Tonyali, C.E. Rogers, Stress-Cracking of Polyethylene in organic liquids, Polymer (Guildf). 28 (1987) 1472–1477.

[16] M. Rink, R. Frassine, P. Mariani, G. Carianni, Effects of detergent on crack initiation and propagation in polyethylenes, Elsevier Masson SAS, 2003. https://doi.org/10.1016/S1566-1369(03)80087-0.

[17] K. Tonyali, H.R. Brown, On the applicability of linear elastic fracture mechanics to environmental stress cracking of low-density polyethylene, Journal of Materials Science. 21 (1986) 3116–3124. https://doi.org/10.1007/BF00553345.

[18] P. Chang, J.A. Donovan, Detergent assisted stress cracking in low density polyethylene, Polymer Engineering & Science. 30 (1990) 1431–1441. https://doi.org/10.1002/pen.760302204.

[19] A.K. Saad, H.A. Abdulhussain, F.P.C. Gomes, J. Vlachopoulos, M.R. Thompson, Studying the mechanism of biodiesel acting as an environmental stress cracking agent with polyethylenes, Polymer (Guildf). 191 (2020) 122278. https://doi.org/10.1016/j.polymer.2020.122278.

[20] J.J. Cheng, M.A. Polak, A. Penlidis, Influence of micromolecular structure on environmental stress cracking resistance of high density polyethylene, Tunnelling and Underground Space Technology. 26 (2011) 582–593. https://doi.org/10.1016/j.tust.2011.02.003.

[21] A.L. Ward, X. Lu, Y. Huang, N. Brown, The mechanism of slow crack growth in polyethylene by an environmental stress cracking agent, Polymer (Guildf). 32 (1991) 2172–2178. https://doi.org/10.1016/0032-3861(91)90043-I.

[22] W. Brostow, M. Fleissner, W.F. Müller, Slow crack propagation in polyethylene: determination and prediction, Polymer (Guildf). 32 (1991) 419–425. https://doi.org/10.1016/0032-3861(91)90444-N.

[23] R.P. Brown, Testing plastics for resistance to environmental stress cracking, Polymer Testing. 1 (1980) 267–282. https://doi.org/10.1016/0142-9418(80)90010-0.

[24] X. Lu, N. Brown, A test for slow crack growth failure in polyethylene under a constant load, Polymer Testing. 11 (1992) 309–319. https://doi.org/10.1016/0142-9418(92)90025-7.

[25] A. Lustiger, R.D. Corneliussen, The role of crazes in the crack growth of polyethylene, Journal of Materials Science. 22 (1987) 2470–2476. https://doi.org/10.1007/BF01082132.

[26] A. Lustiger, R.L. Markham, Importance of tie molecules in preventing polyethylene fracture under long-term loading conditions, Polymer (Guildf). 24 (1983) 1647–1654. https://doi.org/10.1016/0032-3861(83)90187-8.

[27] J.J. Cheng, M.A. Polak, A. Penlidis, Polymer network mobility and environmental stress cracking resistance of high density polyethylene, Polymer - Plastics Technology and Engineering. 48 (2009) 1252–1261. https://doi.org/10.1080/03602550903159085.

[28] M.E.R. Shanahan, J. Schultz, The Influence of Spherulitic Size on the Environmental Stress Cracking of Low Density Polyethylene, 1126 (1980) 1121–1126.

[29] S. Bandyopadhyay, H.R. Brown, Evidence of interlamellar failure in environmental stress cracking of polyethylene, Journal of Materials Science. 12 (1977) 2131–2134. https://doi.org/10.1007/BF00561990.

[30] J.J. Cheng, M.A. Polak, A. Penlidis, Phase interconnectivity and environmental stress cracking resistance of polyethylene: A crystalline phase investigation, Journal of Macromolecular Science, Part A: Pure and Applied Chemistry. 46 (2009) 572–583. https://doi.org/10.1080/10601320902851801.

[31] P.D. Frayer, P.P. Tong, W.W. Dreher, The role of intercrystalline links in the environmental stress cracking of high density polyethylene, Polymer Engineering & Science. 17 (1977) 27–31. https://doi.org/10.1002/pen.760170105.

[32] K. Ueberreiter, G. Kanig, Self-plasticization of polymers, Journal of Colloid Science. 7 (1952) 569–583. https://doi.org/10.1016/0095-8522(52)90040-8.

[33] M.E.R. Shanahan, The role of the liquid in environmental stress cracking of polyethylene, Journal of Materials Science Letters. 2 (1983) 28–32. https://doi.org/10.1007/BF00719949.

[34] G.A. Bernier, R.P. Kambour, The role of organic agents in the stress crazing and cracking of poly(2,6-dimethyl-1,4-phenylene oxide), Macromolecules. 1 (1968) 393–400. https://doi.org/10.1021/ma60005a005.

[35] N.P. Khare, K.C. Seavey, Y.A. Liu, S. Ramanathan, S. Lingard, C.C. Chen, Steady-state and dynamic modeling of commercial slurry high-density polyethylene (HDPE) processes, Industrial and Engineering Chemistry Research. 41 (2002) 5601–5618. https://doi.org/10.1021/ie020451n.

[36] T.E. Nowlin, Business and Technology of the Global Polyethylene Industry, 2014.

[37] S. Ronca, Polyethylene, Elsevier Ltd, 2017. https://doi.org/10.1016/B978-0-323-35824-8.00010-4.

[38] S. Bandyopadhyay, H.R. Brown, Studies of Environmental Stress-Crack Propagation in Low-Density Polyethylene., Journal of Polymer Science. Part A-2, Polymer Physics. 19 (1981) 749–761. https://doi.org/10.1002/pol.1981.180190504.

[39] S. Bandyopadhyay, H.R. Brown, Environmental stress cracking of low molecular weight high density polyethylene, Polymer (Guildf). 22 (1981) 245–249. https://doi.org/10.1016/0032-3861(81)90207-X.

[40] ASTM, ASTM D1693.15 - Standard Test Method for Environmental Stress-Cracking of Ethylene Plastics, ASTM International. (2015) 1–11. https://doi.org/10.1520/D1693-15.2.

[41] Y. Zhang, P.Y.B. Jar, S. Xue, L. Han, L. Li, Measurement of environmental stress cracking resistance of polyethylene pipe: A review, ASME 2019 Asia Pacific Pipeline Conference, APPC 2019. (2019) 1–5. https://doi.org/10.1115/APPC2019-7604.

[42] M. Schilling, U. Niebergall, M. Böhning, Full notch creep test (FNCT) of PE-HD – Characterization and differentiation of brittle and ductile fracture behavior during environmental stress cracking (ESC), Polymer Testing. 64 (2017) 156–166. https://doi.org/10.1016/j.polymertesting.2017.09.043.

[43] E. Nezbedová, P. Hutař, M. Zouhar, Z. Knésl, J. Sadílek, L. Náhlík, The applicability of the Pennsylvania Notch Test for a new generation of PE pipe grades, Polymer Testing. 32 (2013) 106–114. https://doi.org/10.1016/j.polymertesting.2012.09.009.

[44] J.J. Cheng, M.A. Polak, A. Penlidis, A tensile strain hardening test indicator of environmental stress cracking resistance, Journal of Macromolecular Science, Part A: Pure and Applied Chemistry. 45 (2008) 599–611. https://doi.org/10.1080/10601320802168728.

[45] L. Kurelec, M. Teeuwen, H. Schoffeleers, R. Deblieck, Strain hardening modulus as a measure of environmental stress crack resistance of high density polyethylene, Polymer (Guildf). 46 (2005) 6369–6379. https://doi.org/10.1016/j.polymer.2005.05.061.

[46] D.J.M. van Beek, R. Deblieck, Strain hardening: An elegant and fast method to predict the slow crack growth behavior of HDPE pipe materials, Society of Plastics Engineers - EUROTEC 2011 Conference Proceedings. (2011).

[47] Y.G. Hsuan, R.M. Koerner, A.E. Lord Jr, Stress-Craking Resistance of High-Density Polyethylene Geomembranes, Journal of Geotechnology Engineering. 119 (1994) 1840–1855.

[48] R.E. Uhrig, Introduction to artificial neural networks, IEEE Explore. (1995) 33–37. https://doi.org/10.1142/9789814583312_0037.

[49] T. Hastie, R. Tibshirani, G. James, D. Witten, An Introduction to Statistical Learning (2nd Edition), Springer Texts. 102 (2021) 618.

[50] S. Albawi, T.A. Mohammed, S. Al-Zawi, Understanding of a convolutional neural network, Proceedings of 2017 International Conference on Engineering and Technology, ICET 2017. 2018-Janua (2018) 1–6. https://doi.org/10.1109/ICEngTechnol.2017.8308186.

[51] S. Indolia, A.K. Goswami, S.P. Mishra, P. Asopa, Conceptual Understanding of Convolutional Neural Network- A Deep Learning Approach, Procedia Computer Science. 132 (2018) 679–688. https://doi.org/10.1016/j.procs.2018.05.069.

Chapter 3. Improving the Consistency in ESCR Testing of Polyethylene: Development of a Novel Heat Notching Technique

Improving the Consistency in ESCR Testing of Polyethylene: Development of a Novel Heat Notching Technique

V. Gritsichine, H. S. Marway, J. Vlachopoulos, M. R. Thompson*

CAPPA-D/MMRI, Department of Chemical Engineering, McMaster University, Hamilton, Ontario, Canada

Submitted to: Polymer Engineering and Science

August 2022

Abstract

This paper explores a novel modification to the Bell Test (ASTM-D1693) for minimizing its variability in failure time by the introduction of heat notching. The new notching technique for assessing environmental stress cracking resistance was evaluated with four different grades of polyethylene and compared to results using the ASTM standard for notching. Differences in both the failure time and the associated variability were witnessed with this technique, evaluated at various annealing conditions between the cold crystallization temperature and crystal melting temperature of a polyethylene. Best results were found using the midpoint temperature between these two conditions for the heated blade. Localized elastic moduli for the notched samples were obtained by force mapping via atomic force microscopy, showing decreased crystallinity content at the point of concentrated stress was favored for more consistent failure times. The work highlights the critical nature of local phase morphology at the notch in the assessment of environmental stress cracking resistance.

3.1 Introduction

Polyethylene extends to almost every aspect of human activity, as it is adaptable to different sectors such as agriculture, oil transport, and food packaging due to its versatile molecular properties [1]. As with many materials, polyethylene-based products have the potential for failure, which can further translate into high costs associated with property and environmental damage. One common cause for long-term failure with polyethylene is environmental stress cracking (ESC), which is the most common mode of failure for buried pipe [2,3]. Under the general circumstance of buried polyethylene pipe, 10-40% of these parts are reportedly believed to fail in service due to ESC [2,3].

Environmental stress cracking is defined as an accelerated cracking phenomenon associated with a stress cracking agent such as surfactants, oils, alcohols, or detergents without producing chemical degradation in the material [2–9]. One of the first tests to rank polymers for their tendency to fail by ESC is ASTM D-1693, well known as the Bell Test. This method is intended for quality control purposes and assesses the performance of 10 bent "U-shape" samples with a controlled notch in the center of each specimen. These samples are kept in a stressed state using a test-specimen holder, which is further placed into a test-tube containing a solution of the standard stress cracking fluid, IGEPAL C0-630 a nonylpheoxy poly(ethyleneoxy) ethanol. Once submerged, concentrated stresses at the imperfection (notch) causes rapid, localized absorption of the stress cracking fluid that consequentially results in an increase in internal stresses around the notched region leading to failure [2,3,8]. The Bell Test, by design, accelerates the onset of failure to allow rating of polyethylene grades for their resistance to this phenomenon within a reasonable span of

time. The environmental stress cracking resistance (ESCR) rating indicates whether a polyethylene grade is suitable for various consumer uses mentioned previously.

This simple quality control test is very popular since it is rapid and inexpensive; however, it faces major concerns with reproducibility. It was found with the Bell Test. as well as other methods for rating environmental stress cracking resistance, that ESC is heavily sensitive to the thermal processing history of samples under study, which is notably linked to increased variability in failure times [10,11]. The distributions of crystalline and amorphous regions in a polyethylene sample are highly influential on the ESC failure mechanism [4,12,13]. The amorphous regions notably allow the ingress and subsequent plasticization by contact to stress cracking fluid [4,14–16]. Conversely, the influence of crystallinity on ESC is far less predictable [14,17,18]. Higher crystallinity content is generally equated to higher amounts of two types of tie molecules, which are linked to the greater integrity of a part and higher ESCR [14,19,20]. However, tie molecules (or crystalline content) cannot alone explain observed ESC in parts, with other crystalline features noted to impact failure times such as the surface area of crystals, spherulite size, and crystal structures [14,17,18,21,22]. Several current studies on various heat treatments such as quenching or annealing of specimens, show that altering the distribution of crystalline and amorphous regions (phase morphology) in a sample can affect bulk polymer properties associated with ESC [11,20,22–25]. However, this information has yet to be used to reduce ESC variability in the Bell Test.

Research into processing and material factors affecting ESC seem to always consider bulk changes to a sample, such as the discussion of crystalline morphology above,

even though the notched region is the primary driver for this accelerated failure mechanism. This is understandable since characterizing material characteristics in such a small region at the notch is quite difficult. However, recent studies revealing absorption of the stress cracking fluid occurs locally at the notch in the Bell Test, diffusing preferentially into the highly stressed region of the bent specimen, suggesting that bulk properties are less important to the outcome of the test [8,9]. The present work, based on this finding, hypothesizes that greater consistency in failure times for the Bell Test is contingent primarily upon achieving a more reproducible local phase morphology at the notched area.

Therefore, the purpose of this study was to explore the relationship between phase morphology in the local region of the notch, controlled by a heat notching technique, on the variability in failure time of different grades of polyethylene being characterized for their environmental stress cracking resistance by the Bell Test. The goal was to develop a new method of specimen preparation for the test, suitable for industrial use.

3.2. Experimental

3.2.1 Materials and Sample Preparation

Four polyethylene grades provided by Imperial Oil Ltd (Sarnia, ON) were analyzed for this study: HDPE HD 8660.29, HD 8760.29, and HD 9830.02, and LLDPE LL 8460.29. These grades provided a wide range of properties including different environmental stress cracking resistance ratings, as drawn from their respective technical data sheets. ESCR ratings (F_{50}), melt flow indexes (MFI), and densities of all polyethylene are given in Table 3.1 per the information by the supplier. All resins were received as pellets and compression molded into square plaques per Procedure C in Annex 1 of ASTM D4703 [26]. The plaques

were further cut into testing strips of 38 mm x 13 mm x 3 mm (thickness) and then left to rest for 48 hours at room temperature before being tested, following ASTM-D1693 [27].

Table 3.1. Summary of polyethylene properties used in the experimental work

Polyethylene Grade	**F_{50} (hours)**	**MFI (g/10 min)**	**Density (g/cm^3)**
HD 8660.29	40	2.0	0.941
HD 8760.29	20	5.0	0.948
HD 9830.02	370	0.3	0.956
LL 8460.29	60	3.3	0.938

3.2.2 Modified Notching Apparatus

A benchtop universal mechanical testing system, Model 3366 (Instron Corporation; Norwood, MA) was adapted to precisely notch polyethylene samples using a heated notching blade. The instrument was setup with its upper holder configured to grip the blade and its lower holder containing the specimen mounting fixture. A stainless-steel razor blade compliant to the ASTM standard was enclosed in a heater connected to a variable voltage transformer to control its temperature. The custom-made specimen mounting fixture is shown in Figure 3.1. The temperature of the blade at the time of each experiment was measured with an Omega Surface Probe Model No. 88002 (Omega Engineering; Norwalk, CT). When its set temperature was reached, the blade was lowered into the specimen at a crosshead speed of 0.5 mm/min until reaching a notch depth of 0.6235 mm, the standard

depth of a notch stated in ASTM-D1693. The notching blade was kept in this position for 6 minutes while the specimen temperature was monitored using a FLIR thermal camera (Model FLIR-E50) until reaching the same temperature as the blade. The thermal camera was subsequently used to assess how quickly the sample cooled immediately after the blade was removed from the specimen. The specimen was then air-cooled, for 24 hours, before use in the Bell Test.

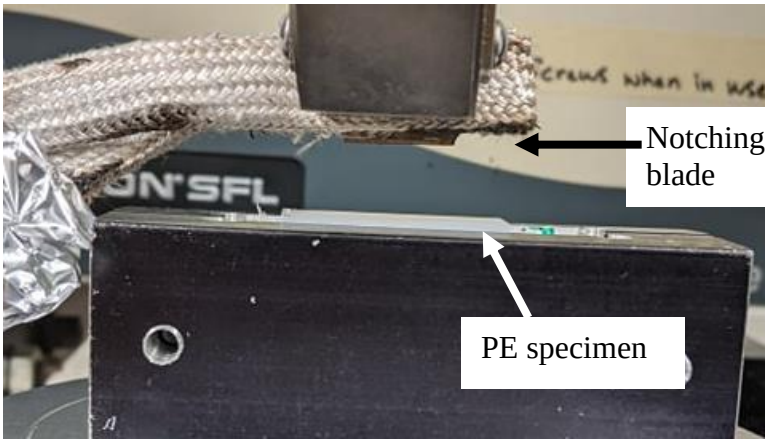

Figure 3.1. Instron Set up for heat notching of polyethylene specimens

3.2.3 Bell Test Preparation and Set-up

Notched specimens were prepared by either the ‘standard method’ using a nicking jig, per ASTM D-1693, or by the ‘heat notching method' as explained above. These specimens were then bent within a 30-second time period and transferred into a brass carrier using a transfer tool, according to ASTM-D1693. Each carrier holding five bent specimens was submerged into a 75 mL glass test-tube containing 10 % IGEPAL CO-630 non-ionic surfactant (Sigma Aldrich; Mississauga, ON) dissolved in Milli-Q purified water; using five rather than ten specimens was required to allow for video monitoring, keeping all specimens within the field of view. The addition of 0.01 wt% of Bromocresol Green (Sigma

Aldrich; Mississauga, ON) to the water was found to suitably track the absorption of the surfactant into the polyethylene specimens. Multiple test-tubes were then placed into a 37.85 L tank heated to 50 °C, controlled by a VWR Signature circulating water bath (VWR International; Mississauga, ON). An Enevox Web Camera with 1280 x 720 pixel resolution and 125 ^{o} viewing angle was mounted in front of the tank to monitor the specimens over time. The camera was controlled by a Python V3.8 coded script to record an image every 10 minutes. Average failure times for specimen were calculated based on the recorded images.

3.2.4 Crystallinity Analysis

Differential scanning calorimetry (model Q200 DSC; TA instruments) was used to determine the crystal melting (T_m) and cold crystallization (T_c) temperatures of the polyethylenes. A sample of 10 mg was weighed and sealed in a Tzero hermetic aluminum pan. A thermogram was collect over a temperature range of 20 °C to 220 °C at a ramp rate of 10 °C/min under a nitrogen purge. The range of notching temperatures tested in this study was based on T_m and T_c for HD 8660.29.

To quantify changes in the phase morphology where the polymer was exposed to the blade during notching, atomic force microscopy (AFM) was used to spatially map the elastic modulus across the area. To conduct the analysis, a failed specimen from the Bell Test was taken and cut down the middle of the notch to expose its two inner surfaces. The inner surface of the notch was further cut into a 2.5 mm x 2.5 mm flat square piece. A TOSCATM^{TM} 400 (Anton Paar Canada; Saint-Laurent, QC) was used with a commercial contact silicon probe with a nominal resonant frequency of 14 kHz and a nominal force

constant of 0.2 N/m. The scan area was confirmed in the AFM system by finding the bromocresol green staining in the monitor. Elastic moduli were calculated for a 50 µm x 50 µm scan area on top of the 2.5 mm x 2.5 mm flat square piece containing the inner surface of the notch using the Tosca^{TM} analysis software (Version 7.4.8341).

3.2.5 Contact Angle

Contact angle was used as an indicator of wettability between the various polyethylene grades with respect to the IGEPAL solution. A failed sample from the Bell Test was dried for at least 24 hrs and then cut down the middle of the notch to expose the two inner surfaces of the notch. Contact angle was measured using the sessile drop method, where an angle was determined from the base to the tangent of the drop curvature. Each drop contained 3 µL of the 10% IGEPAL CO-630 solution and the contact angle was recorded by a computer software program (FTÅ software, First Ten Angstroms, Inc), with image intervals every 5 seconds for 100 seconds using a CCD camera connected to a microscope. The contact angle at 100 seconds was used as the final value. The reported average value for each grade and treatment condition was based on four repeated measurements.

3.2.6 Bending Load Analysis

Bending stresses were assessed for three heat notched specimens at 120 °C and three standard notched specimens, for each grade of polyethylene. Each sample was bent as described in Section 2.3 and then secured in a custom C-Clamp holder that held it against an OMEGA LCM703-10 10 kg load cell (Omega Engineering; Norwalk, CT). This setup

is shown in Figure 3.2. Load was tracked for 15 minutes using an Arduino Uno Rev 3 microcontroller connected to a computer via an HX711-ADC amplifier, with data recorded every 15 seconds. The data obtained was normalized and averaged for three repeats of each condition to produce a singular load curve for each grade of polyethylene.

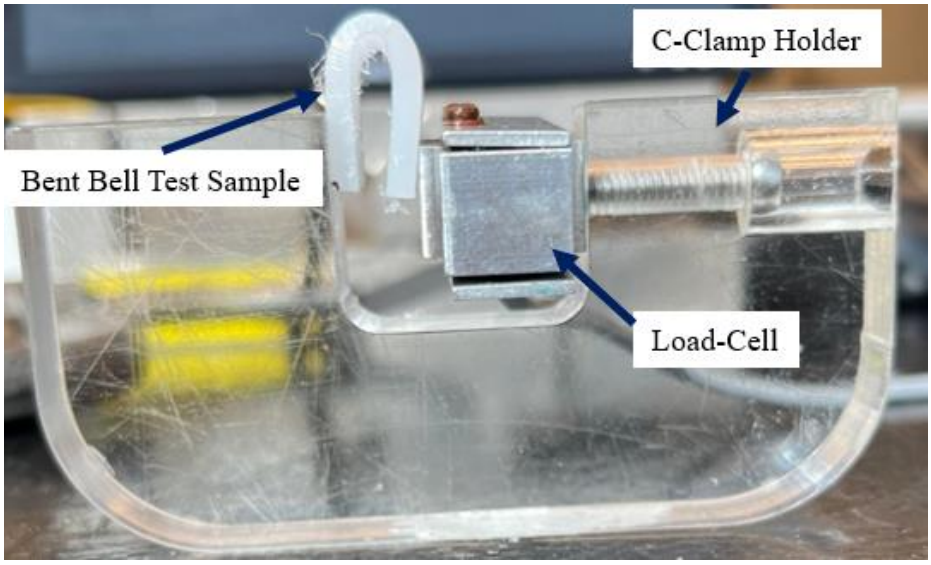

Figure 3.2. Compressive Load Cell Set-Up containing a C-Clamp Holder, Bent Sample providing force against the Load Cell

3.3 Results and Discussion

3.3.1 Developing the heat notching method

The range of blade temperatures used in the study were selected between T_c and T_m for HD 8660.29. In this preliminary trial, heat notching was conducted at 110 °C, 120 °C, and 130 °C and considered two HDPE grades in the evaluation, HD 8660.29 and HD 8760.29. HD 8760.29 had a higher estimated crystallinity (58%) than HD 8660.29 (50%), determined by DSC (using 293 J/g the theoretical value of heat of fusion for the calculation

of 100 % crystallinity [8]). These polyethylene grades were selected for the first tests since they exhibit relatively low failure times, allowing more Bell Tests to be conducted within a reasonable span of time while seeking to understand the influence of annealing locally in the notched area. The results were compared to the standard method of notching where the blade is equilibrated to room temperature (23 °C). Final failure times as well as the variability in failure times are given in Table 3.2, while the respective percent change in these values with respect to the standard method are given in Table 3.3; variability in failure time is reported in this study as the standard deviation for the number of failed specimens. The reported failure time corresponded to the time that the camera recorded a visibly broken specimen; this was not F_{50} as described for the Bell Test in its ASTM standard.

Table 3.2. Results of heat notching in the preliminary trials

Polyethylene Grade	**Notch Temperature (°C)**	**Failure Time (Hours)**	**Number of Failed Samples**
HD 8660.29	Room Temperature	42.53 ± 2.78	9
HD 8660.29	110	71.72 ± 10.39	9
HD 8660.29	120	44.85 ± 1.85	9
HD 8660.29	130	142.08 ± 31.56	4
HD 8760.29	Room Temperature	12.09 ± 2.39	6
HD 8760.29	110	10.81 ± 0.92	6

HD 8760.29	120	12.75 ± 1.49	6
HD 8760.29	130	16.24 ± 3.33	6

Table 3.3. Percent change in failure time and variability in the preliminary trial

Polyethylene Grade	**Notch Temperature (°C)**	**Percent Change in Failure time (%)**	**Percent Change in Variability (%)**
HD 8660.29	110	69	274
HD 8660.29	120	5	-33
HD 8660.29	130	234	1053
HD 8760.29	110	-11	- 62
HD 8760.29	120	5	-38
HD 8760.29	130	34	39

At the notching temperature of 110 °C, HD 8660.29 specimens showed an increase in failure times by 69% when compared to the standard method, while variability increased by 274%. Comparatively, HD 8760.29 showed the opposite behavior with a reduction in both failure time and variability by 11% and 62%, respectively. A similar outcome for variability and failure times of specimens was seen at the notching temperature of 130 °C for both HD 8660.29 and HD 8760.29 samples. Conversely, variability in failure time was reportedly lower at 120 °C while the failure times at this temperature remained on par with samples tested by standard notching, for both polyethylene grades. Since reduced

variability was the focus of the study, these results at this mid-point temperature condition were preferred.

Use of a thermal camera allowed the flow of heat to be observed during and after the notching process. Thermograms captured immediately after the blade was removed are shown in Figure 3.3 for the three elevated notching temperatures. Radiant heat was only detected in the notch at 110 °C whereas by 130 °C, the heat associated with notching was noted up to 1-2 mm beyond the location of the blade. Overall, the influence of the heated blade was restricted to the notch area but notching at 120 ^{o}C and 130 ^{o}C appeared to be more likely to anneal polymer further from the blade surfaces. The temperature of the notch area decreased rapid upon removal of the heated blade, with recorded values taken approximately 5 s afterwards shown in Table 3.4. Each polyethylene sample showed immediate cooling, decreasing by 40 °C in a very short span of time.

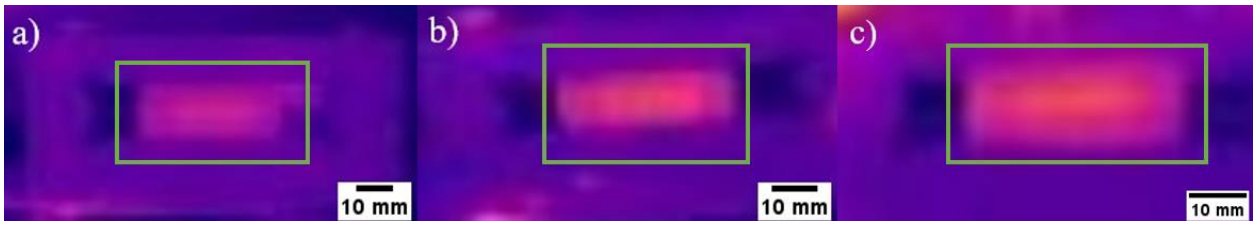

Figure 3.3 Thermograms of the notch (highlighted by a green box) right after the application of heat notching a) 110 °C, b) 120 °C, c) 130 °C

Table 3.4. Thermal camera measurements post heat notching

Polyethylene Grade	Notch Temperature (°C)	Thermal Camera Reading (°C)
HD 8660.29	110	57.16 ± 4.02
HD 8660.29	120	79.00 ± 5.36
HD 8660.29	130	94.83 ± 7.00
HD 8760.29	110	60.33 ± 3.08
HD 8760.29	120	77.33 ± 4.42
HD 8760.29	130	89.33 ± 4.36

The extreme temperature conditions for heat notching corresponded too closely to the transitional crystalline states for these polymers to positively alter the influential phase to affect stress development during the Bell Test. This was reasonably determined as the best annealing condition found between these two boundaries in terms of altering the phase morphology of the polymer at the notch. An interesting finding between the two extremes was the opposing trends seen between the two similar polymers. At 110 °C, chain mobility was the most restricted for the studied temperature range but sufficient for crystalline rearrangement. The increase in time as well as standard deviation found for HD 8660.29 was indicative of larger crystal lamella being produced along with a higher chance of inter-lamellar linkages [14,17]. Conversely, the results with the lower molecular weight HD 8760.29, with its higher crystallinity, pointed to only minor crystalline reorganization and a reduction in tie molecules [23]. These different responses highlight the sensitivity of the

Bell Test to even minor differences in crystallinity at the notch, which correspondingly affect failure times. At 130 °C, chain mobility was much greater and specimens were often prone to experience undesirable melt flow away from the heated blade. These notched samples often included long and thin fibrils that would emerge from the notched area while being bent, as seen in Figure 3.4a. Furthermore, the dye added to the IGEPAL solution produced the least discoloration of the notch by heat notching at 130^{o}C compared to any other tested condition including the standard method. Major increases in crystallinity were produced in both polymers, creating a beading and stringing effect that could impede both absorption and stress development. Due to the increases in crystallinity around the notched area, there was a reduction of amorphous content allowing for a decreased absorption of IGEPAL CO-630 into the notched area, highlighted by the reduction of the dye around the surface area in direct proximity to the notch, as seen in Figure 3.4b-f. With the reduced capacity of absorption, the crystalline content present could sustain stresses from the fluid as well as bending forces for a longer period, thus delaying failure times. This was indicated in both HD 8660.29 and HD 8760.29 by their longer failure times.

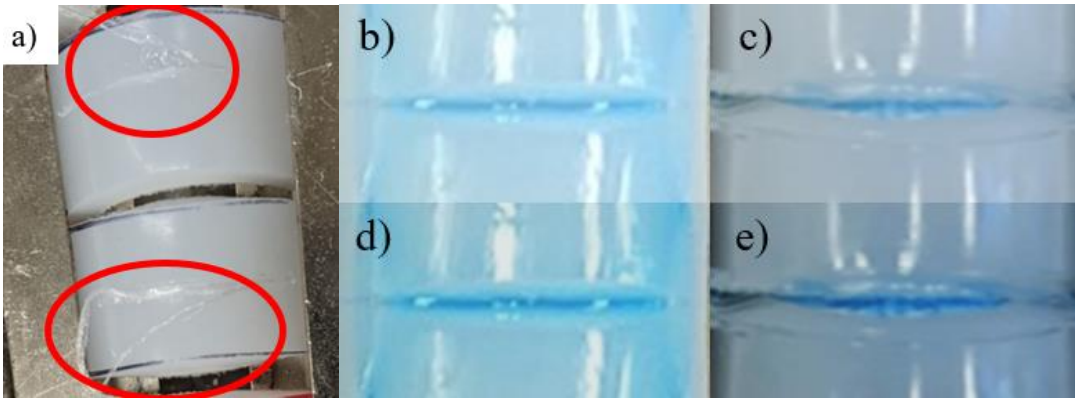

Figure 3.4. Physical findings of Notching at 130 °C a) Fraying of heat notched sample when bending highlighted by the red ovals b) Standard Method of Notching c) 130 °C Notch, d) Standard Method of Notch (-20% Brightness, +40% Contrast), e) 130 °C Notch (-20% Brightness, +40% Contrast)

With an increase in variability and possibly failure time, blade temperatures of 110 °C and 130 °C were deemed to be unsuitable for future studies on the heat notching technique. However, the 120 °C condition provided sufficiently promising results for reducing the variability in the failure time to merit more detailed study with a broader range of polyethylenes in regard to ESCR. Additionally, notching at this temperature did not produce the long and thin threads, nor did it produce any melt flow at the notch, which was preferred for not producing new defects in the notch region to complicate stress development.

3.3.2 Comparison of the Modified Bell Tests and Original Bell Test

The two additional polyethylenes considered now in the tests were a bimodal molecular weight HDPE (HD 9830.02), and a linear low-density polyethylene with narrow molecular weight distribution (LL 8460.29). These two polyethylenes exhibited much more varied characteristics compared to the first two, as seen in Table 3.1, and were chosen to highlight grades with large variability of failure time, which is usual for higher F_{50} values. All four polymers were tested (or re-tested) with the 120ºC notching temperature and with a greater number of specimens. Table 3.5 summarizes the failure times, and Table 3.6 summarizes the percent change in failure time (and variability) between standard and heat notching.

Table 3.5. Failure times for the four grades of polyethylene comparing heat notching at 120 °C to the standard method

Polyethylene Grade	**Temperature (°C)**	**Failure Time (Hours)**	**Number of Samples Tested**
HD 8660.29	Room Temperature	49.69 ± 7.22	16
HD 8660.29	120	46.99 ± 5.54	21
HD 8760.29	Room Temperature	13.34 ± 3.84	19
HD 8760.29	120	12.59 ± 2.43	19
HD 9830.02	Room Temperature	130.72 ± 33.50	25
HD 9830.02	120	114.14 ± 21.32	27
LL 8460.29	Room Temperature	54.84 ± 9.32	21

LL 8460.29	120	53.39 ± 6.14	18

Table 3.6. Percent change in failure time and variability (based on standard deviation) comparing heat notching versus the standard method

Polyethylene Grade	**Percent Change in Failure Time (%)**	**Percent Change in Variability (%)**
HD 8660.29	-5	-23
HD 8760.29	-6	-30
HD 9830.02	-13	-36
LL 8460.29	-3	-34

Overall, with notching at 120 °C, failure times were found to reduce by 3-13% (which was an unintended consequence but still considered a positive outcome since testing could now be shorter) and variability in failure time decreased by 23-36% compared to standard notching. A consistent improvement in variability was seen for all polyethylenes, whether short or long in failure time, unaffected by the broad differences in structures tested. The annealing during notching was considered to be relieving residual stresses related to the molding of specimens [28–31] and reducing the specimen-to-specimen differences in their phase morphology within the notch where the stress cracking agent was preferentially being drawn during the Bell Test. The relieved residual stresses were observable through the measured stresses of bent specimens, shown in Figure 3.5 for heat notched and standard notched samples. Only the first 15 minutes of stresses were reported,

as being more representative of the initial state of the bent specimen before significant molecular rearrangement related to the stress cracking agent could occur. It was consistently found that heat notched samples exhibited a lower stress in their initial bent state over the standard method of notching, by ~19-26% for most grades but by 69% for HD 8660.29. The next section examines the phase morphology at the notch to explain these findings.

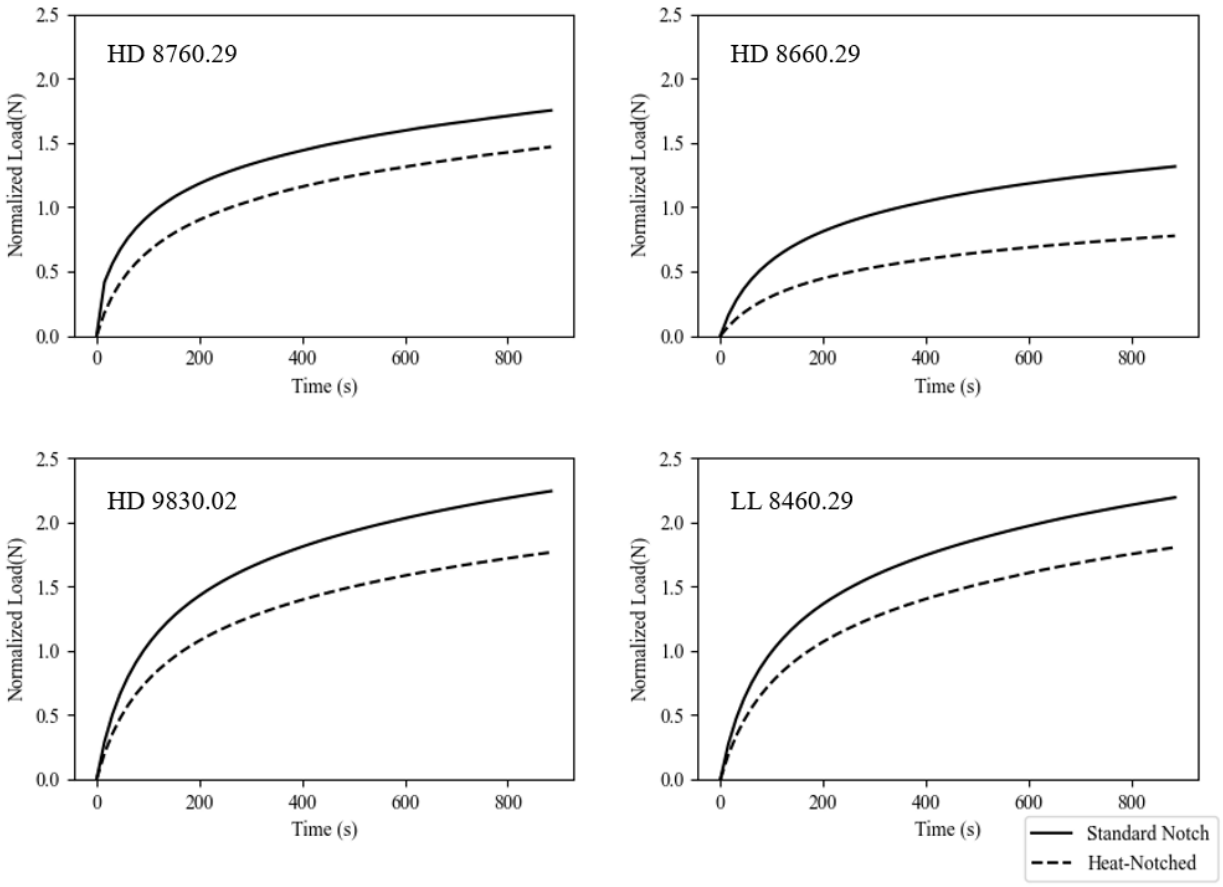

Figure 3.5. Normalized Load (N) over 15 minutes immediately after bending, for all four polyethylene grades

3.3.3. Evaluation of the notched region

To understand the changes in the notch due to annealing, AFM was used to map the local elastic moduli within its inner surfaces. Figure 3.6 presents spatial contour plots to visualize the change in stiffness locally for HD 8860.29 (F_{50} = 40 h, Table 3.1) versus HD 9830.02 (F_{50} = 370 h, Table 3.1). In both cases, there appeared to be an increase in the amorphous phase because of heat notching, signified by the decreased elastic moduli over the majority of the scanned sections. The remaining hard domains in the scanned surface appeared smaller in size for the heat notched specimens compared to the standard notched specimens. The changed crystallinity associated with these hard domains was specifically localized to the surfaces of the notch and could not be detected by DSC when we attempted to microtome a thin layer off the sample for analysis. This seems consistent with the thermograms of Figure 3.3 which indicate the heating effect by the blade was local to the surfaces of the notch.

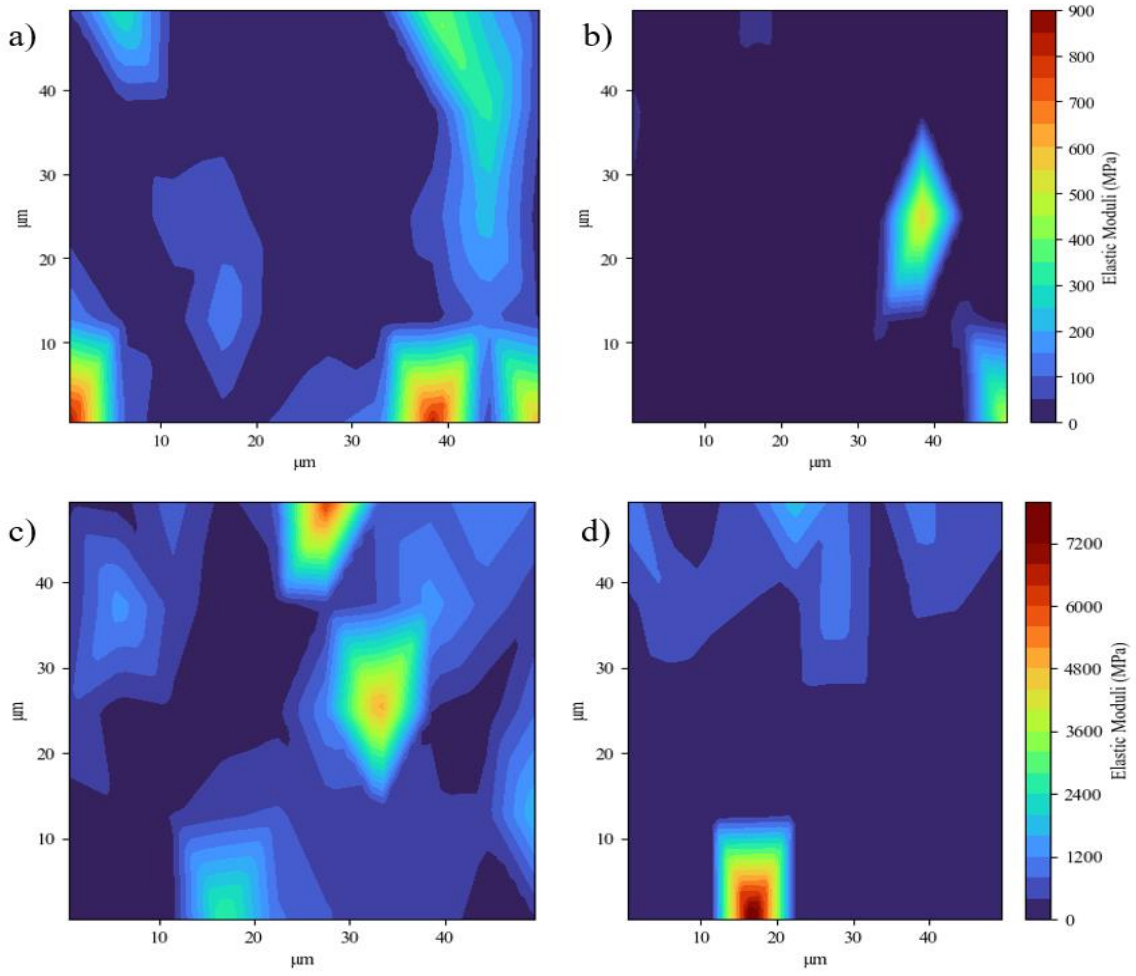

Figure 3.6. Spatial Elastic Moduli Mapping of HD 8660.29, a) Standard Notch and b) Heated Notch, and HD 9830.02, c) Standard Notch, and d) Heated Notch

The exposed surfaces of the notch were tested for changes in wettability by measurement of the contact angle for each polyethylene grade, as given in Table 3.8. The characterization was challenging to perform on such small areas, resulting in some specimens yielding no stable angle values. Among the samples notched at room temperature (standard method), HD 9830.02 and LL 8460.29 exhibited lower contact angles than HD 8660.29 and HD 8760.29. Samples after heat notching showed a decline in

contact angle in comparison to the standard method, albeit negligibly for HD 9830.02. The change could have been caused by oxidative degradation, though new functional groups in such a localized area will be too low in concentration to be confirmed by FTIR. However, considering the robust stabilizer package used in HD 8660.29 (a grade targeted for rotational molding), which should have effectively resisted such chemical reactions, it seemed more likely that the contact angle change was linked to the phenomena noted by AFM regarding reduced hard domains content. Metal substrates (including steel) have been noted in other studies to act as nucleating agents for polyethylenes, initiating transcrystallization at contacting interfaces, especially at elevated temperatures where the contact (wetting) is greater despite surface roughness [32–34]. The noted impact on the polymer in such cases was a reported decrease in the contact angle. Considering a suppressed size of crystals due to enhanced nucleation would appear as a reduction in hard domains at the surface contacting the heated notching blade and the resulting decrease in contact angle seen in our testing, attributing nucleation to explain the influence of the notching blade on the response of the polyethylene seems most plausible. Regardless of the cause, the reduced contact angles seen for heat notched samples would benefit IGEPAL CO-630 wettability, allowing for better opportunities for localized absorption to occur along the notched surface. However, while resins with lower hydrophilicity experienced higher ESCR in this study there was no observable correlation between contact angle and failure time; the only significant factor correlated with ESCR in this study was melt flow index.

Table 3.8. Summary of contact angles of IGEPAL CO-630 solution – polyethylene grades tested

Polyethylene Grade	Contact Angle (°)	
	Standard	**Heat Notched**
HD 8660.29	28.86 ± 3.00	12.31*
HD 8760.29	32.33 ± 4.71	21.87 ± 6.6
HD 9830.02	17.49 ± 3.58	16.19 ± 0.43
LL 8460.29	20.19 ± 4.28	N/A *

*Samples were not successfully tested

A roughness map via AFM for standard and heat notched samples can be seen in Figure 3.7. The representative inner notched surface appeared smoother using the heated blade. This can be seen through the histogram within the plots produced, showing that the heat notched samples had a uniform distribution of height when compared to the standard notch. The smoother surface would be less prone to the concentrating of stresses during the Bell Test, contributing to the longer failure time. The smoother surface might also be related to the lower contact angle values seen above since rougher surfaces are more prone to appear hydrophobic, although this is not a simple relationship, being dependent on peak-to-valley height differences and the frequency of peaks [35]. It is therefore plausible that roughness and surface chemistry are influencing the absorption of IGEPAL CO-630 and stress development during the Bell Test, though the changes in phase morphology seemed to be the largest change by heat notching.

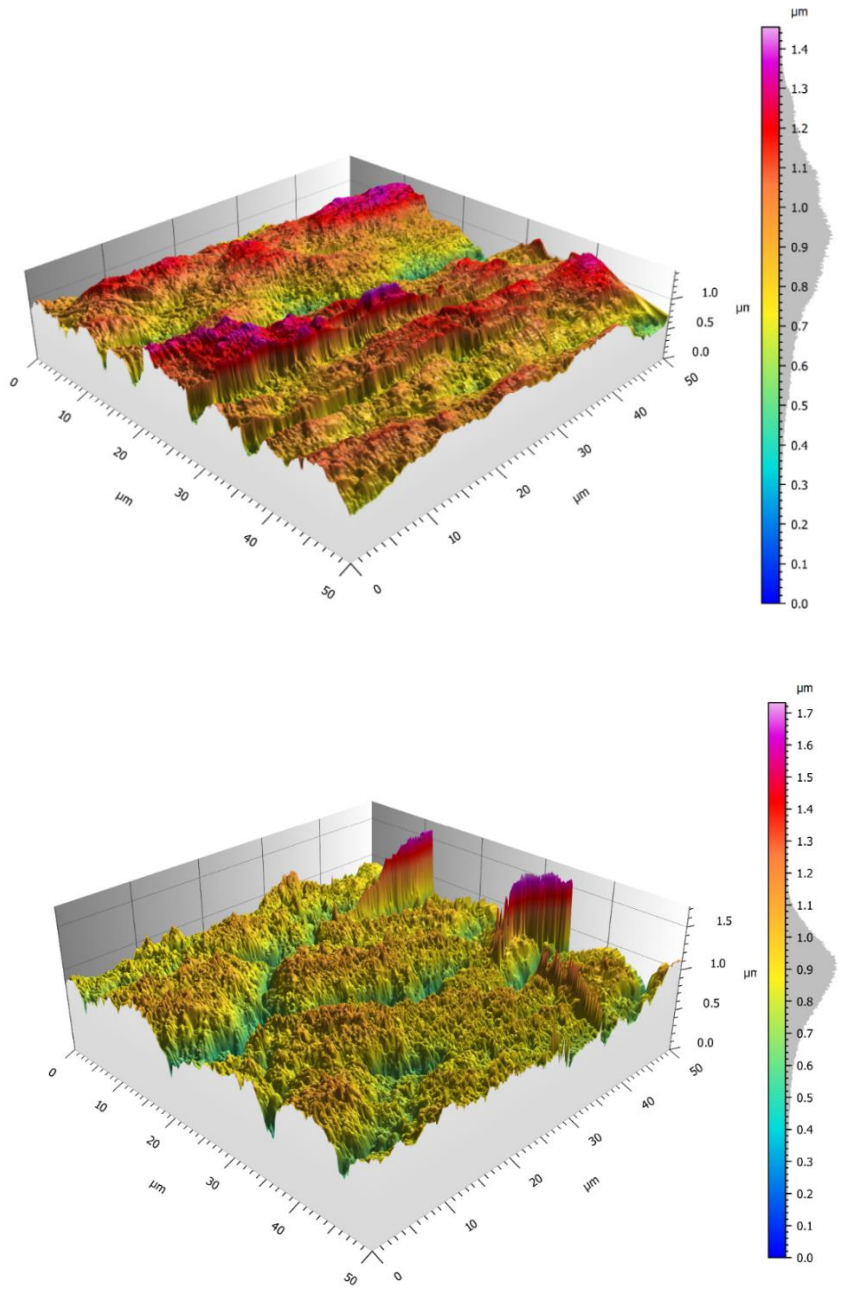

Figure 3.7. Reconstructed Three-Dimensional Inner Surface Notch View of HD 8660.29 by the Standard method (top) and Heat Notching method (below) mapped using AFM

3.3.4. General Discussion

The resultant phase morphology found by AFM with heat notching pointed to reduced crystallinity in the newly notched surfaces and a reduction in size of the remaining crystals. There will be a corresponding decline in associated tie molecules and interlamellar linkages by this change, which can be related to the lowering of bending stresses found in the prepared specimens. The relative decline in bending stresses by heat notching was largest for HD 8660.29, which could be the reason that its failure times were least likely to decrease and often increased. However, since failure times were generally reduced by heat notching among the four polyethylenes in the test, despite the decline in stresses, the change in phase morphology was considered to have the greater effect on the participation of IGEPAL CO-630 on the crack growth mechanism. The greater apparent amorphous content at the notch surface allowed IGEPAL CO-630 to be preferentially drawn into the bent polyethylene sample; the dye showed impeded absorption of the surfactant when crystallinity was allowed to form to a greater degree, notably at 130 °C in the preliminary tests. The heat of the blade did not appear to penetrate deeply into the polymer and since attempts to analyze changes in crystallinity by DSC failed to see the change, it is reasonable to consider the higher apparent amorphous content found by AFM was localized to the surfaces of the notch. Based on this observation, these notch surfaces offered less resistance to the ingress of the surfactant than under standard conditions, but the polymer offered no significant change in its capacity to absorb more of the plasticizer. Since failure times and their variability were reduced by heat notching despite lower bending stresses, the more rapid absorption of IGEPAL was felt to be important to this outcome. The

outcome could be as simple as the earlier absorption of the stress cracking agent accelerating the test. The decrease in contact angle as well as smoothness of heat notched samples should also be considered as secondary factors that favorably contributed to the overall improved ingress of IGEPAL into the bent specimen.

Inherently, variability in failure times is considered to be dependent upon all elements of the Bell Test where repeatability cannot be assured, not just for the preparation of test specimens. However, crystallization is likely the least controllable element in the test, especially for polymers of broad molecular weight distribution, making the present approach to be a simple solution to the variability in the test.

3.4. Conclusion

Annealing was investigated at the notch surfaces of polyethylene to decrease its variability of failure times as well as the failure times themselves in the Bell Test. Notching at the cold crystallization temperature was found to increased failure times and variability, which was attributed to the higher crystalline content. Notching at the crystal melt temperature produced increased disturbances such as fraying around the notch as well as a beading effect impeding stress development within the notch which yielded delayed failures and increased variabilities. The optimal heat notching temperature was found between the cold crystallization temperature and melting temperature, with a notable increase in reproducibility caused by a reduction in crystallinity and its associated structures such as tie-molecules and interlamellar linkages. The altered phase morphology due to heat notching was very local to the surfaces of the notch, thought to aid IGEPAL

CO-630 absorption into the semi-crystalline structures beneath the amorphous surface layer. The heat notched samples exhibited lower residual stresses as bent specimens and yet the failure times were lower in the Bell Test. Through contact angle measurements and roughness measurements by the AFM, it was seen that the heat notched samples provided for higher surface energies as well as smoother surfaces, resulting in the improved wettability of IGEPAL CO-630 on the notched surface. This further equated to an increased opportunity for IGEPAL CO-630 to diffuse into the notched surface quicker then the standard method of notching. In return the notch was able to experience a quicker uptake of stress-cracking fluid allowing for quicker and less variable failure times.

3.5. Acknowledgements

The authors would like to thank Imperial Oil Ltd. for their funding of this work. The authors would like to especially thank Ron Cooke at Imperial Oil for his advice, supply of materials, and technical discussions throughout the development of the heat notching technique. We would further like to thank Mohammad Shariful Islam Chowdhury at the McMaster Manufacturing Research Institute (MMRI) for assisting with Atomic Force Microscopy, and finally Hassan Abdulhussain and Austin Bedrosian at McMaster University for their helpful insights during the initial stages of the development of the heat notching technique.

References

[1] M. Demirors, The History of Polyethylene, 2011. https://doi.org/10.1007/978-1-4614-6504-1_1.

[2] M. Schilling, Environmental Stress Cracking (ESC) and Slow Crack Growth (SCG) of PE-HD induced by external fluids, (2019).

[3] D. Wright, Environmental Stress Cracking of Plastics, 1st ed., Rapra Technology Limited, 1996.

[4] K. Tonyali, C.E. Rogers, Stress-Cracking of Polyethylene in organic liquids, Polymer (Guildf). 28 (1987) 1472–1477.

[5] K. Tonyali, H.R. Brown, On the applicability of linear elastic fracture mechanics to environmental stress cracking of low-density polyethylene, Journal of Materials Science. 21 (1986) 3116–3124. https://doi.org/10.1007/BF00553345.

[6] M. Rink, R. Frassine, P. Mariani, G. Carianni, Effects of detergent on crack initiation and propagation in polyethylenes, Elsevier Masson SAS, 2003. https://doi.org/10.1016/S1566-1369(03)80087-0.

[7] N. Ogata, T. Yanagwa, K. Yoshida, Environmental Stress Cracking of Low-density Polyethylene in Normal Alcohols, 24 (1986) 89–97.

[8] A.K. Saad, H.A. Abdulhussain, F.P.C. Gomes, J. Vlachopoulos, M.R. Thompson, Studying the mechanism of biodiesel acting as an environmental stress cracking agent with polyethylenes, Polymer (Guildf). 191 (2020) 122278. https://doi.org/10.1016/j.polymer.2020.122278.

[9] A.K. Saad, F.P.C. Gomes, M.R. Thompson, Plasticizing effect of oxidized biodiesel on polyethylene observed by nondestructive method, Fuel. 252 (2019) 246–253. https://doi.org/10.1016/j.fuel.2019.04.122.

[10] R.P. Brown, Testing plastics for resistance to environmental stress cracking, Polymer Testing. 1 (1980) 267–282. https://doi.org/10.1016/0142-9418(80)90010-0.

[11] X. Lu, N. Brown, Effect of thermal history on the initiation of slow crack growth in linear polyethylene, Polymer (Guildf). 28 (1987) 1505–1511. https://doi.org/10.1016/0032-3861(87)90350-8.

[12] S. Bandyopadhyay, H.R. Brown, Studies of Environmental Stress-Crack Propagation in Low-Density Polyethylene., Journal of Polymer Science. Part A-2, Polymer Physics. 19 (1981) 749–761. https://doi.org/10.1002/pol.1981.180190504.

[13] H.R. Brown, A theory of the environmental stress cracking of polyethylene, Polymer (Guildf). 19 (1978) 1186–1188. https://doi.org/10.1016/0032-3861(78)90069-1.

[14] J.J. Cheng, M.A. Polak, A. Penlidis, Influence of micromolecular structure on environmental stress cracking resistance of high density polyethylene, Tunnelling and Underground Space Technology. 26 (2011) 582–593. https://doi.org/10.1016/j.tust.2011.02.003.

[15] F.P.C. Gomes, W.T.J. West, M.R. Thompson, Effects of annealing and swelling to initial plastic deformation of polyethylene probed by nonlinear ultrasonic guided waves, Polymer (Guildf). 131 (2017) 160–168. https://doi.org/10.1016/j.polymer.2017.10.041.

[16] F.P.C. Gomes, A. Bovell, G.P. Balamurugan, M.R. Thompson, K.G. Dunn, Evaluating the influence of contacting fluids on polyethylene using acoustic emissions analysis, Polymer Testing. 39 (2014) 61–69. https://doi.org/10.1016/j.polymertesting.2014.07.007.

[17] J.J. Cheng, M.A. Polak, A. Penlidis, Phase interconnectivity and environmental stress cracking resistance of polyethylene: A crystalline phase investigation, Journal of Macromolecular Science, Part A: Pure and Applied Chemistry. 46 (2009) 572–583. https://doi.org/10.1080/10601320902851801.

[18] P. Hittmair, R. Ullman, Environmental stress cracking of polyethylene, Journal of Applied Polymer Science. 6 (1962) 1–14. https://doi.org/10.1002/app.1962.070061901.

[19] S. Bandyopadhyay, H.R. Brown, Evidence of interlamellar failure in environmental stress cracking of polyethylene, Journal of Materials Science. 12 (1977) 2131–2134. https://doi.org/10.1007/BF00561990.

[20] P.D. Frayer, P.P. Tong, W.W. Dreher, The role of intercrystalline links in the environmental stress cracking of high density polyethylene, Polymer Engineering & Science. 17 (1977) 27–31. https://doi.org/10.1002/pen.760170105.

[21] S. Bandyopadhyay, H.R. Brown, Environmental stress cracking and morphology of polyethylene, Polymer (Guildf). 19 (1978) 589–592. https://doi.org/10.1016/0032-3861(78)90287-2.

[22] M.E.R. Shanahan, J. Schultz, The Influence of Spherulitic Size on the Environmental Stress Cracking of Low Density Polyethylene, 1126 (1980) 1121–1126.

[23] S. Bandyopadhyay, H.R. Brown, Environmental stress cracking of low molecular weight high density polyethylene, Polymer (Guildf). 22 (1981) 245–249. https://doi.org/10.1016/0032-3861(81)90207-X.

[24] M.J. Shirkavand, H. Azizi, I. Ghasemi, M. Karabi, Effect of Molecular Structure Parameters on Crystallinity and Environmental Stress Cracking Resistance of High-Density Polyethylene/TiO2 Nanocomposites, Advances in Polymer Technology. 37 (2018) 770–777. https://doi.org/10.1002/adv.21719.

[25] J.M. Lagaron, N.M. Dixon, W. Reed, J.M. Pastor, B.J. Kip, Morphological characterisation of the crystalline structure of cold- drawn HDPE used as a model material for the environmental stress cracking (ESC) phenomenon, Polymer (Guildf). 40 (1999) 2569–2586. https://doi.org/10.1016/S0032-3861(98)00500-X.

[26] ASTM International, Standard Practice for Compression Molding Thermoplastic Materials into Test Specimens, Plaques, or Sheets, (2016) 1–13. https://doi.org/10.1520/D4703-16.2.

[27] ASTM, ASTM D1693.15 - Standard Test Method for Environmental Stress-Cracking of Ethylene Plastics, ASTM International. (2015) 1–11. https://doi.org/10.1520/D1693-15.2.

[28] B. Chen, H. Yang, K. Shen, Q. Fu, X. Gao, The effect of high-temperature annealing on thermal properties and morphology of polyethylene pipes prepared by rotational shear, Polymer (Guildf). 204 (2020) 122770. https://doi.org/10.1016/j.polymer.2020.122770.

[29] J.S. Kim, J.H. Yoo, Y.J. Oh, A study on residual stress mitigation of the HDPE pipe for various annealing conditions, Journal of Mechanical Science and Technology. 29 (2015) 1065–1073. https://doi.org/10.1007/s12206-015-0218-7.

[30] G. Lebrun, J. Denault, Effect of annealing on the thermal expansion and residual stresses of bidirectional thermoplastic composite laminates, Composites Part A: Applied Science and Manufacturing. 41 (2010) 101–107. https://doi.org/10.1016/j.compositesa.2009.09.009.

[31] D. Chen, B. Wang, H. Wang, S. Wang, K. Ni, L. Zheng, H. Zhang, H. Qi, J. Shao, Effect of thermal annealing on a cuboid DKDP crystal, Journal of Alloys and Compounds. 817 (2020) 152812. https://doi.org/10.1016/j.jallcom.2019.152812.

[32] H. Schonhorn, Heterogeneous nucleation of polymer melts on high-energy surfaces. II. Effect of substrate on morphology and wettability, Macromolecules. 1 (1968) 145–151. https://doi.org/10.1021/ma60002a008.

[33] K.M. Seven, J.M. Cogen, J.F. Gilchrist, Nucleating Agents for High-Density Polyethylene - A Review, Polymer Engineering and Science. 56 (2016) 541–554. https://doi.org/10.1002/pen.

[34] F.L. Binsbergen, Natural and Artificial Heterogeneous Nucleation in Polymer Crystallization., J Polym Sci Polym Symp. 29 (1976) 11–29. https://doi.org/10.1002/polc.5070590104.

[35] Z. Li, K. Liao, F. Liao, Q. Xiao, F. Jiang, X. Zhang, B. Liu, C. Sun, G. Chen, Wetting and Spreading Behaviors of Nanodroplets: The Interplay among Substrate Hydrophobicity, Roughness, and Surfactants, Journal of Physical Chemistry C. 120 (2016) 15209–15215. https://doi.org/10.1021/acs.jpcc.6b04299.

Chapter 4. Focusing our Understanding of Environmental Stress Cracking in the Bell Test on the Notch Region

Focusing our understanding of environmental stress cracking in the Bell Test on the notch region

V. Gritsichine, J. Vlachopoulos, M. R. Thompson*

CAPPA-D/MMRI, Department of Chemical Engineering, McMaster University, Hamilton, Ontario, Canada

Submitted to: Engineering Fracture Mechanics

September 2022

ABSTRACT

The Bell Test (ASTM-D1693) is commonly used to accelerate failure in order to evaluate resin selection for applications like piping and tanks where environmental stress cracking is possible, even though the method offers less than desirable repeatability. The working hypothesis for this new study with polyethylenes was that the variability seen in failure times is attributed to a high sensitivity to the phase morphology primarily at or near the surfaces of a notch, affecting stresses and the localized absorption of the preferred stress cracking agent, moreso during the test than the more commonly referenced bulk descriptors of a polymer. Using an organic dye tracer to monitor penetration of stress cracking agent into the polymer along with image analysis for the notch dimensions and a load cell, the local aspects of the mechanism were evaluated for up to four grades of polyethylene of varying crystallinity. By this detailed analysis, it was revealed that for failure to occur by ESC, influences in the polymer by absorption of the stress cracking agent preceded the changes in stresses in the specimen, contrary to original expectation. There was an imminent rate increase in both stresses and notch expansion once absorption of the surfactant reached a critical concentration. This critical nature was shown to be dependent on the crystallinity of the polymer under observation, considering the size/arrangement of crystals present and entanglements formed through the amorphous contents to dictate the rate by which IGEPAL can be absorbed into a polyethylene specimen. The results of this study validate the need for greater focus on polymer properties at the notch rather than the bulk of the specimen, though more techniques for providing analysis of these properties at the notch surfaces are needed for future improvements to the mechanism.

4.1. Introduction

Environmental stress cracking (ESC) is defined as the acceleration of stress cracking for a polymer part merely by its contact with a fluid in the absence of chemical degradation [1–4]. The mechanistic behaviour of ESC is therefore purely physical. A broad range of fluids are identified as stress cracking agents capable of accelerating stress cracking, including soaps, wetting agents, oils, and detergents [1–7]. These fluids adsorb, absorb, and plasticize polymers like polyethylene, influencing craze initiation, crack growth and the eventual fracture of a part subject to small yet prolonged stresses [1–4,6] .

Various studies conducted over the years have explored environmental stress cracking resistance (ESCR) of polyethylenes through the lens of engineering its physical properties using various co-monomers, polymerization catalysts, and thermal processing techniques [8–16] . The structural changes produced by these factors led to differences in either crystallinity or the molecular entanglements between crystalline regions [8,11,17–24]. Researchers have found many interrelated descriptors, such as spherulitic size, tie molecules, inter-lamellar linkages, lamella surface areas, which can dramatically affect ESC [6,8,20,24]. These co-dependencies result in a non-linear relationship between phase morphology and ESC in determining ESCR ratings. It is thought that these changes in crystalline structure vary the polymer's resistance to stress cracking fluid absorption, or its strength to resist against ESC failure, or both, resulting in variable failure times.

Only certain fluids appear to magnify existing stresses acting upon a polyethylene part when absorbed, decreasing its failure time [1,6]. Polymer-fluid interactions within this

setting for environmental stress cracking are therefore considered to be as important as the polymer's phase morphology in the resistance of a material to failure. Current literature shows that the role of the stress cracking fluid in the failure mechanism is dependent upon its diffusion into the amorphous polyethylene phase [7,20,25,26]. The sorption of this fluid local to the defect is driven by an increase in surface interaction energies and lowering of the polymers surface tension to the stress cracking fluid [1,7,25]. The imbalanced net force resulting from the subsequent plasticization drives the craze-crack mechanism that leads to the disassembling of tie molecules, breakage of the crystalline structure and the ultimate fracture of the part [8,20,27]. Bulk crystalline properties of a polymer are often related to the absorption of stress cracking fluids in the literature.

Recent studies have brought into question the importance of a bulk description of the polymer for ESCR assessment compared to a more focused consideration of the notch itself. This new viewpoint arose with a study of biodiesel as a stress cracking fluid, which because of its yellow color made it possible to visually observe the preferential (almost exclusive) absorption of the stress cracking agent into the notch region of Bell-Test specimen as ESC occurred [7]. This observation was felt to be the first indication that environmental stress cracking, at least in the Bell Test, was much more sensitive to the polymer state at the surfaces of the notch than previously conceived. However, this viewpoint brings significant challenges for evaluation since most direct analysis techniques will quantify much more of the surroundings than may be affecting the ESC mechanism. We believe there is acute sensitivity to the local phase morphology at the notch that causes the large variability seen in the Bell Test. Given the significance of a stress cracking fluid

on the failure mechanism, this local environment may be better understood by this fluid's sorption into a polymer specimen relative to local stresses and the amorphous/crystalline phase morphology present at this point of ingress. To consider this new viewpoint, this work examines the ESC behaviour of various polyethylene grades containing different crystallinity. To validate this local sensitivity, several characterization techniques are developed in this study and evaluated for their effectiveness.

4.2. Experimental

4.2.1. Materials

Four polyethylene grades were provided as pellets by Imperial Oil LTD (Sarnia, ON), namely two high density grades, HDPE (ExxonMobil^{TM} HD 8660.29, HD 9830.02), a linear low-density grade, LLDPE (ExxonMobil^{TM} LL 8460.29), and an experimental grade LA080. These four grades provided a broad range of ESCR ratings, as listed in their technical data sheets provided by the resin supplier. A summary of properties consisting of ESCR rating (F_{50}, per ASTM-D1693), density, melt flow index (MFI), and crystallinity percentage for all tested grades can be seen in Table 4.1. Square plaques of each resin were compression molded following Procedure C in Annex 1 of the ASTM-D4703 [28]. Once molded, plaques were cut into test specimens with dimensions of 38mm x 13mm x 3mm (thickness), as suggested by the ASTM-D1693 [29]. In some instances, under a modified Bell Test, longer specimens were cut into 65mm x 12.5mm x 3mm (thickness) strips instead. Following the preparation of the Bell-Test specimen, these samples were left to rest for 48 hours at room temperature before undergoing testing. The grades HD 9830.02

and LA080 were used for the initial analysis of the organic dye tracer. In-depth analyses of the interactions between the stress cracking fluid and polyethylene were conducted with HD 8660.29 and LL 8460.29. The choices were made based on F_{50} and the differing amorphous and crystallinity phase morphology in the polyethylenes.

4.2.2 Crystallinity Analysis

To determine crystallinity percentages of all polyethylene grades used in this study, differential scanning calorimetry (model Q200 DSC; TA Instruments) was used to determine the crystal melting temperature (T_m). Additionally, HD 8660.29 and LL 8460.29 samples which have failed by the Bell Test were assessed by the DSC for their crystallinity percentage. To conduct the crystallinity percentage of failed samples, the Bell Test specimens were cut down the middle of the notch to expose the two inner surfaces. Both inner surfaces of the notch were used in the DSC analysis, combined together to make 10 mg. Samples of HD 8660.29, HD 9830.02, LL 8460.29, and LA080 were tested within the DSC and consisted of 10 mg. All samples were then sealed in a Tzero hermetic aluminum pan and a thermogram was collected over the temperature range of 20°C to 220°C at a ramp rate of 10°C/min under a nitrogen purge. The percentage of crystallinity was calculated based on the measured enthalpy of the melting transition as well as the theoretical heat of fusion for a 100% crystalline polyethylene (293 J/g) [7].

Table 4.1. Summary of Polyethylene Properties

Polyethylene Grade	Density (g/cm^3)	MFI (g/10 min)	ESCR (F_{50} Hours)†	Crystallinity Percentage* (%)
HD 8660.29	0.941	2.0	40	50
HD 9830.02	0.956	0.30	370	68
LL 8460.29	0.938	3.3	60	44
LA080	0.955	0.35	48	61

† supplied by the resin vendor

* measured at the notch of bent specimens

4.2.3. ESCR testing procedure

Specimens were notched by a nicking-jig highlighted in the ASTM D-1693 standard. After the samples were notched, the specimens were bent over a 30 second period and then transferred into a brass carrier via the use of a transfer tool highlighted in the standard. Each carrier contained five bent specimens which were immersed in a 75 mL glass test-tube containing the stress cracking fluid, 10% IGEPAL CO-630 (Sigma Aldrich; Mississauga, ON) dissolved in Milli-Q purified water with 0.01 wt% Bromocresol Green dye. In the instances that required the modified Bell Test, the modified Bell Test specimen was notched and bent into a U-shape using modified tools intent on the same purpose as those described in the ASTM standard. The modified Bell Test was used in conjunction with studies relating to the testing of various degrees of bending forces shown in Section 4.2.4. Test-tubes containing either standard or modified test specimens were then placed in a 38 L tank heated by a VWR Signature circulating water bath heater (VWR International; Mississauga, ON) set to 50°C.

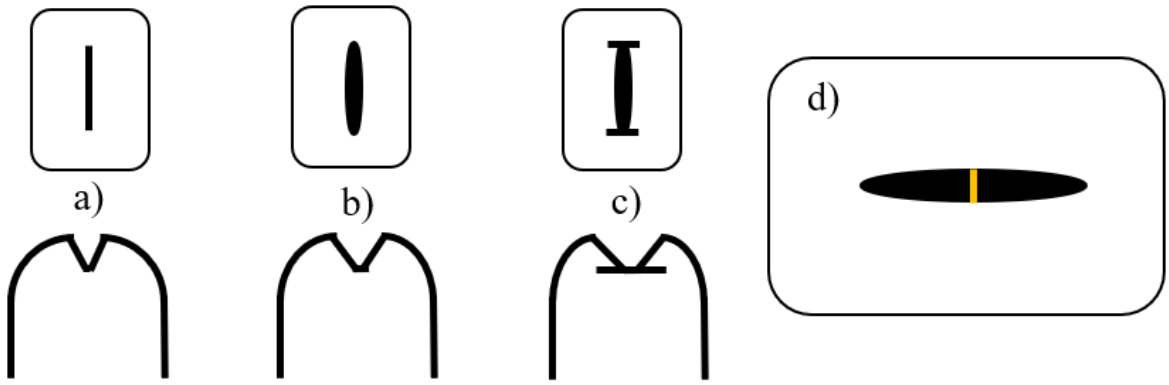

Figure 4.1. Notch Dilation throughout testing, a) Start of Test, b) Halfway throughout testing, c) Completion of testing, d) Specimen containing a dilated notch, where the yellow line highlights the top-down view of the cross-section measured for notch dilation

Notch dilation is a measure of the width of the notch (transverse to the direction of the cut surface) over the duration of the Bell Test, which is graphically depicted in Figure 4.1. The sample number per carrier for each trial was reduced from the standard ten samples to only five samples in order to record all notches simultaneously for their measurement on an hourly basis; the recording mentioned involved the carrier being taken out of a test tube and photographed, with all five samples captured in a single image. Notch dilation was recorded until the failure of all five samples occurred.

The trend in notch dilation showed two stages, starting with a period of slow widening (lag period) and then accelerated growth in size. A previous study has noted the same trend [30]. This transition period was determined by calculating the minimum of the first derivative and is further referred to in this study as ‘IGEPAL’S Transition Time’.

Comparatively, this method arose from the determination of the point at which a transition in slopes occurs, consequentially synonymous with the end of the lag period. The transition between the two stages is not abrupt, in general, and so two methods were considered for quantifying the representative transition time for the measured parameter enduring heightened effects from IGEPAL, in this case notch dilation. In the first approach, the trend in the logarithmic transformed data was analyzed by two best-fit simple lines applied to the lag and accelerated stages respectively. The intersection time shared by the two linear functions is called 'IGEPAL Acceleration Time' (or just acceleration time). The second approach relied upon fitting the data to a logistic growth model, even though the model includes a final stage of declining rate of change that was not seen in the data of this study and thus reduced the goodness of fit at higher test times. The logistic growth model has three fitted variables, a, b, and c, as seen in Eqn (4.1). The estimated time of the transition in this case corresponded to the time found in Eqn (4.2) at which a maxima occurs for the first derivative of Eqn (4.1) and called 'Time of IGEPAL Acceleration'. This point is the time at which the steepest upward slope within the data.

$$\text{Logistic Growth Model } Notch\ Dilation\ (mm) = \frac{a}{1+b(e^{-cx})} \tag{4.1}$$

$$\text{Time of IGEPAL Acceleration } \textit{(hours)} = \frac{\ln\left(\frac{a}{\frac{ab}{2}}\right)}{-c} \tag{4.2}$$

The Time of IGEPAL acceleration was similarly determined in the same manner for the color parameter and stress intensity factor K, both described in Sec. 4.2.4 and 4.2.5 below. This was done by usage of the Gradient function found in Numpy's Python Library.

4.2.4. Use of a color dye as tracer of the stress cracking fluid

Bromocresol Green (Sigma Aldrich; Mississauga, ON) was chosen as a tracer for IGEPAL CO-630 absorption into our polyethylene specimens during the Bell Test, since the surfactant is transparent and could not be visually tracked by itself, unlike the previous findings with biodiesel [7]; the color parameter used to imply IGEPAL absorption is described in Section 4.2.5. To validate the chosen dye's effectiveness for tracing surfactant absorbed into the polyethylene specimens, preliminary studies were conceived whereby different stresses at the notch were created to produce different driving forces for absorption of IGEPAL. Notched specimens made of HD 8660.29, had holes drilled into both ends and were bent to different angles, held in place using copper wire sewn through the holes. These specimens were individually immersed into jars containing either 10% IGEPAL CO-630 solution with 0.01 wt% Bromocresol Green added or only 0.01 wt% Bromocresol Green in Milli-Q water. The jars were placed into a VWR Signature circulating water bath (VWR International; Mississauga, ON) at 50°C for 72 hours.

Bromocresol Green exhibited a color change (from green to blue) after approximately the first 20 hours in the Bell Test. To assess the cause, polyethylene samples and the brass carrier used in the test were separately submerged into a 10% IGEPAL CO-630 mixture containing 0.01wt% Bromocresol Green. Each test-tube was submerged in a VWR Signature circulating water bath at 50 ^{o}C for 1 hour and then visually inspected for color change. Details as to the cause of the color change will be discussed in Section 4.3.1.

4.2.5. Modified ESCR testing procedure

To carry out a detailed study evaluating bending stresses simultaneously with notch dilation and surfactant absorption (color parameter), a modified setup was required that considered only one notched specimen at a time. The environmental aging conditions were comparable to the Bell Test. A standard-compliant bent and notched Bell Test specimen was placed inside a custom C-Clamp holder containing a load cell, using the transfer tool highlighted in ASTM-D1693. The specimen was kept bent by being clamped against the load cell, with its notch area immersed in a 10% IGEPAL CO-630 solution with 0.01wt% Bromocresol Green dye. The solution was kept at 50°C, monitored by a K-Type OMEGA HH11C Thermometer (Omega Engineering; Norwalk, CT). A layer of silicon oil was applied atop of the IGEPAL CO-630 mixture to minimize evaporation since the system had to be left open to atmosphere on account of the electronics. This set up is schematically shown in Figure 4.2.

Load data corresponding to the bent specimen was collected by an Arduino Uno Rev 3 microcontroller that was connected to an OMEGA LCM703-10 10 kg load cell (Omega Engineering; Norwalk, CT) via a HX711-ADC amplifier. The load data was transformed into bending stresses using bending inertial moments as well as the area moment of inertia. These two factors were used to calculate the bending stress developing in the material. The bending stress was used to calculate the *stress intensity factor K* [31], as an estimate of the residual stresses at the notch during a Bell Test. This approach provides a single parameter descriptor of the bending stresses by assuming a one-dimensional finite plate consisting of uniform uniaxial stresses, which was used to describe

the notched surface of a test specimen. Once the stress intensity factors were calculated for each sample, the data was further smoothed using a one-dimensional Gaussian Filter provided by SciPy's Python library.

Notch dilation and absorbed surfactant concentration for the test specimen was determined using an Enevox Web Camera containing a 120° viewing angle that was positioned under the glass container holding the solution, looking upwards at the notched face of a bent specimen. The camera recorded an image every 10 minutes via a custom Python V3.8 script. The same method for collection notch dilation data was used as described in Section 4.2.3. The value of RGB color pixels within the notch (area being preferably dyed during the Test) was divided by the RGB color value at outer edge of the notch (relatively uncolored area) to calculate the 'color parameter'. An example of how the color parameter was extracted from images is seen in Figure 4.2. This color parameter was monitored simultaneously with the measured stresses and notch dilation data. The plotted color parameter data shown in this paper were smoothed using a Savitzky-Golay filter found in the SciPy Python library. Smoothing was necessary due to ambient lighting within the testing room fluctuating throughout the day creating a slow oscillation in the plotted results.

The Time of IGEPAL Acceleration and IGEPAL Transition time (Section 4.2.3) were used in this test to analyze the change in rate for notch dilation, color parameter and stress intensity factor K. A minimum of three repeats was used in this assessment.

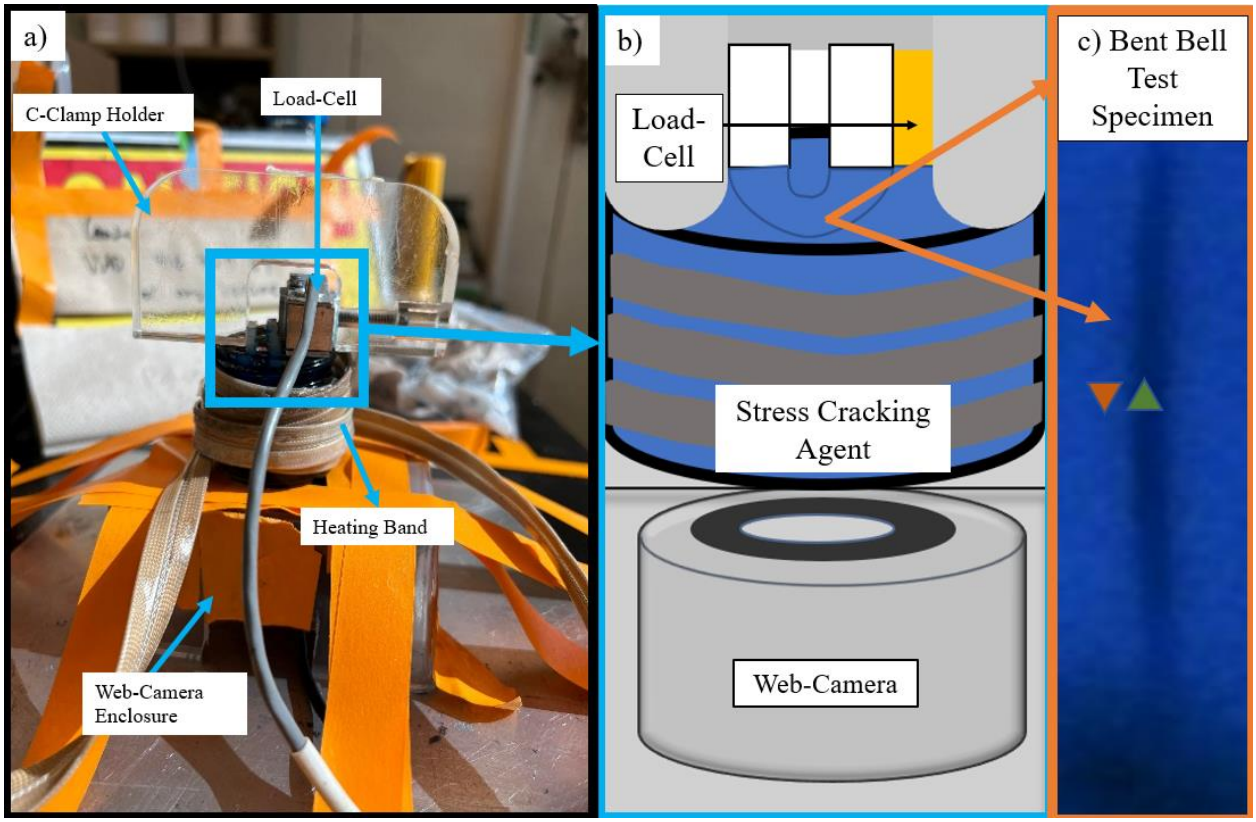

Figure 4.2. Set-up for the modified ESCR test: **(a)** photo from the lab, (b) schematic for the setup, and (c) close-up image of the notch seen by the web camera, with the spatial locations used to calculate the color parameter highlighted (green triangle for the pixel coordinates inside of the notch versus the orange triangle indicating the coordinates used outside of the notch).

4.3. RESULTS AND DISCUSSION

4.3.1. Use of a dye tracer in the Bell Test

As previously mentioned, a study found that the inherent yellow color of biodiesel as a stress cracking agent allowed researchers to track its absorption into the test specimen during the Bell Test [7]. Over the course of a test trial, grades of polyethylene prone to ESC developed an intense yellow discoloration that was exclusively present at the notch

that was found to correspond to the intensification of internal stresses over time. All other areas of the bent specimen showed little or no coloring by the end of the test. These observations suggested at the time that the influence of a stress cracking agent may be almost exclusively at the defect site if their absorption only occurred due to ESC. However, due to limited user access to this fluid and the delayed failure times associated with its use in the Bell Test, biodiesel was not considered a viable replacement for IGEPAL CO-630 surfactant. Unfortunately, the clear color of the preferred stress cracking fluid, IGEPAL CO-630, in the ASTM standard provides little means of directly corroborating these findings with biodiesel and direct analysis of its absorption into a specimen by FTIR (using attenuated total reflection of failed specimens at the notch) does not detect such low concentrations. Consequently, a visual tracer for the surfactant was sought whose discoloration of polyethylene specimens could be directly related to the concentration of surfactant absorbed. Additionally, the ideal tracer should not significantly influence the failure time of polymers in the Bell Test.

Through initial testing of many different colored fluids added to water, Bromocresol Green dye was found to be most suitable as the ideal tracer. Bromocresol Green is an organic dye typically used as a pH indicator between 3-5, changing from yellow in an acidic solution to deep blue in a more basic solution. In the Bell Test setup, an aqueous solution (with or without IGEPAL CO-630 present) containing the dye changed from green to deep blue in a matter of hours, which was eventually attributed to oxidation in the presence of the brass carrier used in the Bell Test. As a result, all staining of polyethylene samples was blue rather than green in color, as shown in Figure 4.3. Subsequently, the nature of this

dye as a tracer was examined by varying its concentration in the aqueous solution containing immersed bent polyethylene (LA080) test specimens, with and without 10% IGEPAL CO-630 included.

Figure 4.3. Coloration of washed and dried LA080 specimens after 48 h immersed in the solution containing a)10% IGEPAL CO-630 without Bromocresol Green, or 10% IGEPAL CO-630 with Bromocresol Green at concentrations of b) 0.0005 wt%, c) 0.005 wt%, d) 0.01 wt%, e) 0.025wt%, f) 0.05 wt%.

As a trial for the Bell Test progressed (data not shown), concentrations of the dye between 0.0005 – 0.025wt% allowed the notch in the specimen to remain visible while specimens were still immersed, which was important for future experiments to develop a real-time visual monitoring method for the Bell Test. At 0.05 wt% dye and above, a notch could not be observed while immersed in the solution during a Bell Test trial. After the polyethylene specimens were removed from these different dyed solutions, this coloring was persistent and could not be rinsed or wiped from the specimens (as seen in Figure 4.3).

Notch staining in the removed polyethylene specimens was difficult to distinguish for dye concentrations between 0.0005 – 0.005 wt%; some coloring was visibly seen by eye at the notch but its quantification in the camera images was not reliable. A suitable concentration range for the dye was found between 0.01wt% and 0.025wt%, considering the trade-offs between visibility of specimens while immersed in the solution versus the intensity of blue coloring in polyethylene specimens removed for the imaging used for the results sections below. For the rest of the study, a tracer concentration of 0.01 wt% Bromocresol Green was used as the ideal.

In the absence of IGEPAL CO-630, as seen in Figure 4.4, 0.01 wt% dye showed no significant sorption into the specimens as evident by the absence of any detectable blue discoloration observed. In this case, the test had been extended up to 552 hours and we considered all four polyethylene grades, with no evidence of staining in any specimen when the surfactant was not included in the solution. Bromocresol Green did not, in this case, show any tendency to act as a stress cracking agent by itself nor did this dye show any influence on IGEPAL CO-630 as a stress cracking agent in repeated ESCR testing with LA080 (based on the failure times). It was found that with the inclusion of various Bromocresol Green concentrations in ESCR testing with LA080, the same F_{50} value of 40 hours was achieved as the case without its use.

Figure 4.4. Washed and dried polyethylene test specimens immersed in a 0.10 wt% Bromocresol Green solution, a) HD8660.29 (552 hours), b) LL8460.29 (552 hours), c) LA080 (552 hours), d) HD9830.02 (168 hours)

Finally, to confirm whether the tracer/IGEPAL solution was being drawn into the polyethylene specimens by concentrated stresses at the notch associated with the test, as previously seen with biodiesel, altered specimens with varying degrees of bend were studied. Images of the altered Bell Test specimens (HD 8660.29) of varying angles, after 48 hours of immersion, are shown in Figure 4.5. Only specimens with a bending angle greater than 143.5 degrees exhibited coloring around the notch and in both conditions, fracturing was eventually observed to indicate the stresses needed to be high enough in the 48-hour period to produce stress cracking. Specimens with a lower bending angle exhibited no coloration change at the notch and did not fail.

The association of Bromocresol Green with IGEPAL CO-630 in the test system was its inclusion within micelles of the surfactant; sorption of a surfactant into polyethylene specimens for various ESCR test methods has been consistently described as micelle migration in the literature [4–6]; an organic dye being incorporating in micelles has also been observed in non-ESCR studies [32]. The presence of the micelle was critical for dye absorption into the polymer else it had no direct means of sorption, as noted by the lack of staining when no surfactant was included in the test solution. With this tracer dye, IGEPAL CO-630 sorption behavior could now be studied in the same manner as found with biodiesel [7] despite the surfactant concentration in polyethylene being too low for reliable detection by other means of chemical analysis (like FTIR). The intensity of blue color seen in the notched area is treated in the subsequent sections as the concentration of absorbed surfactant over the duration of the Bell Test.

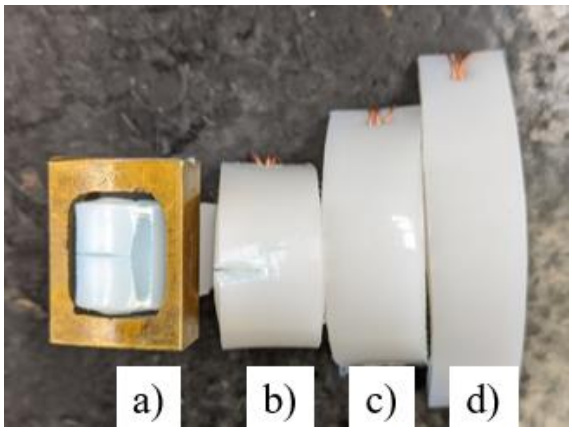

Figure 4.5. Coloring and cracking of specimens with a bending angle of a) 168.3°(matching the Bell Test), b) 143.5°(high bend), c) 120.8°(medium bend), d) 89.6°(low bend)

4.3.2 Failure analysis at the notch

4.3.2.1 Notch Dilation Analysis

Observing notch dilation served as a direct means of failure analysis for the accelerated ESC in the Bell Test. This metric is similar to the well-known crack opening displacement metric, used to track samples undergoing fatigue testing [33]. The measured expansion of the notch displayed two inherent behaviors over the course of a Bell Test, shown in Figure 4.6 for HD 8660.29 and LL 8460.29; both resins were selected for this preliminary study since their failure times are characteristically short (around 2 days) which allowed for many repeats and faster changes in the methodology as it was developed. The two behaviors were more readily seen on a logarithmic scale. Early expansion of the notch appeared steady in rate but then increased in dilation rate as specimen fracturing was imminent. The two behaviors for notch gap width are highlighted in the plots by manually identifying the two log-log data sets based on the trend and then linearly regressing each group of data. The calculated *IGEPAL acceleration time* where the two lines cross was 20.2 hours and 26.1 hours for HD 8660.29 and LL 8460.29, respectively, increasing with the vendor-reported F_{50} value for the two polymers. However, since the transition between the two stage was not abrupt but rather, gradual, a second approach to quantifying the two stages was considered in the hopes to see cause/effect relations once the color parameter and bending stresses are likewise considered. The failure times of HD 8660.29 and LL 8460.29 were 60.34 ± 17.81 hours and 56.26 ± 15.95 hours, indicating a 29.5% and 28.3% percentage variance in failure times for HD 8660.29 and LL 8460.29 respectively.

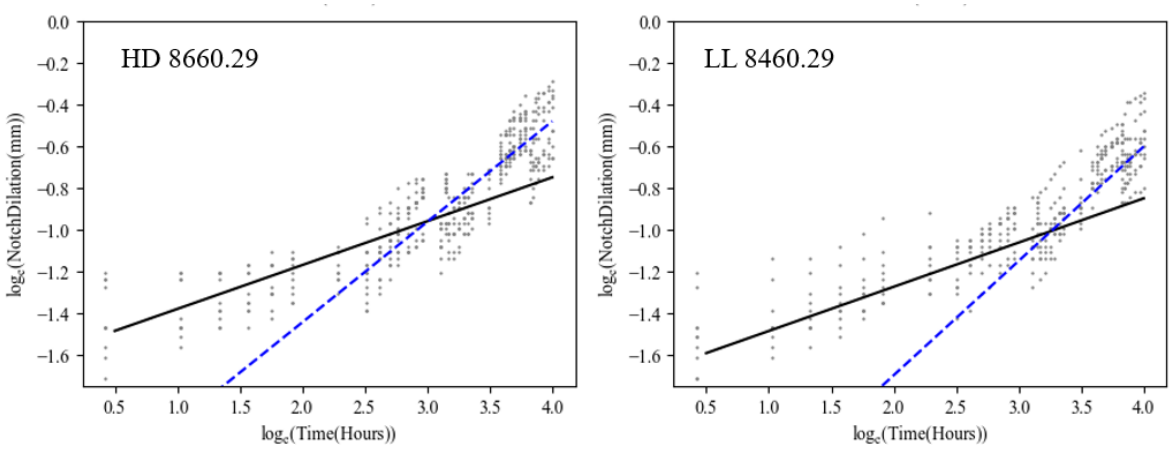

Figure 4.6. Notch dilation over time for HD 8660.29 and LL 8460.29 tested in a 10% IGEPAL CO-630 solution containing 0.01 wt% Bromocresol Green tracer. Black line reflects the lag stage while the dashed blue line represents the accelerated growth stage.

To comprehensively describe all data collected over a test, without manual selection of the data groups, a fitted logistic growth model was found to encompass the two dilation behaviors seen at the notch. The quality of fit can be seen in Figure 4.7. The Time of IGEPAL Acceleration (TIA) calculated as 22.0 hours and 27.5 hours, for HD 8660.29 and LL 8460.29 respectively. These values appear very close to the IGEPAL acceleration time and thus were treated as equivalent. These different approaches along with the minima of the first derivative, known as IGEPAL Transition Time in the literature are summarized in Table 4.2 for the two polymers.

Table 4.2. Comparison of different methods to identify the transition between the rate of notch dilation seen during a Bell Test trial.

Grade of Polyethylene	IGEPAL Transition Time, hours (*Ln*(hour))	IGEPAL Acceleration Time, hours (*Ln*(hour))	Time of IGEPAL Acceleration, hours (*Ln*(hour))	End of Test, hours (*Ln*(hour))
HD 8660.29	2.36 ± 1.14	3.25 ± 0.93	3.09 ± 1.41	4.10 ± 2.88
LL 8460.29	2.38 ± 0.80	3.20 ± 0.88	3.31 ± 1.35	4.03 ±2.77

Reflecting on the tabulated results compared to the plotted data, the IGEPAL transition time identifies the end of the lag stage, the IGEPAL acceleration time reflects the midway point in the transition, and the time of IGEPAL acceleration give the start time of exclusively accelerated growth; a key difference between the transition time and the time of acceleration for notch dilation is that the latter is an indicator of yielding as well as the onset of micro-voids forming at the notch tip, fitting the observations of Thuy et al and Yeh et al [34,35]. Among the three qualifiers of the transition, the acceleration time was considered the most arbitrary based on the need to identify the two data groups and thus, led to concerns over repeatability especially when testing times are increased for some grades of polyethylene.

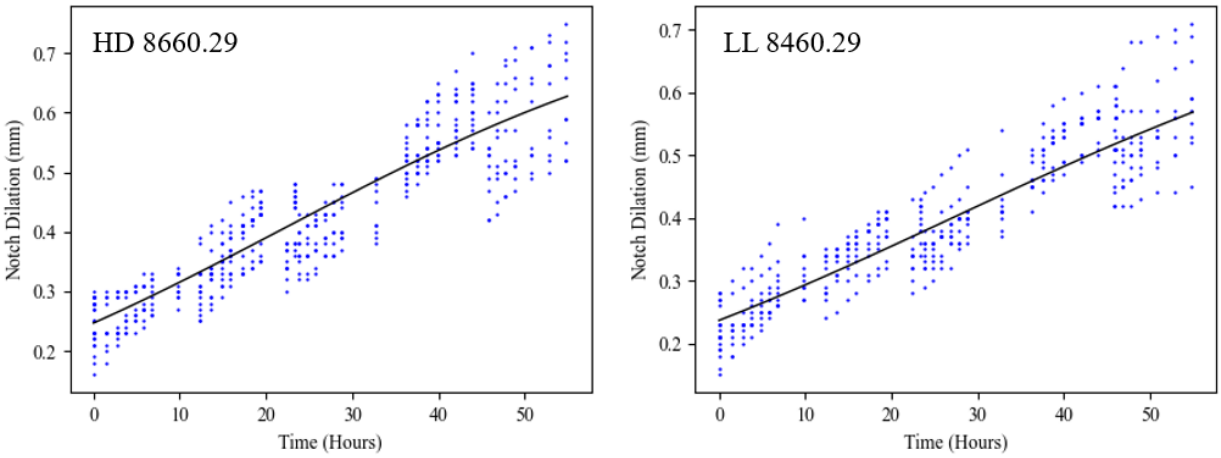

Figure 4.7. Notch dilation over time for HD 8660.29 and LL 8460.29 tested in a 10% IGEPAL CO-630 solution containing 0.01 wt% Bromocresol Green tracer. Black lines reflect the Logistic Growth Model (HD 8660.29 R^2 = 0.81, LL 8460.29 R^2 = 0.82), while the blue points reflect the raw data.

4.3.2.2 Surfactant absorption and stress analysis

Theorized models on ESC highlight the importance of surfactant absorption and stresses on the polymer to explain crack growth and eventual part failure. To examine the coincidence of bending stresses (associated with the load cell setup) and absorbed surfactant concentration (determined by the color parameter value in the area of the notch) with respect to notch dilation over the duration of the Bell Test, a modified setup was required to collect all of these values simultaneously. It was seen for both grades of polyethylene that testing times in the modified setup were approximately ~2.5 times longer than in the standard Bell Test, as the average failure times for HD 8660.29 and LL 8460.29 for the modified set up were 101.66 ± 13.64 and 171.5 ± 81.26 hours respectively.

It is seen that LL 8460.29's failure times held a higher failure time as well as standard deviation in comparison to HD 8660.29. The independent failure times of LL 8460.29 for the three samples were 169.66, 311.33, 171.5 hours. Comparatively, the second sample held roughly a ~ 2 times higher failure time then the other two samples, thus skewing the IGEPAL Transition and Acceleration time standard deviations shown in Table 4.3. The percentage variance of both HD 8660.29 and LL 8460.29 were 13% and 47% respectively within the modified Bell Test set up. The average of percentage variation of failure times along the two grades consisted of 30%. Comparatively in the unaltered Bell Test seen in the previous section, the percentage variance was on average 30%. Therefore, when comparing the percentage variance of failure time in the previous section and the percentage variance of failure within this section, the modified Bell Test set up failure times consisted of an ±15% of variance within failure times of individual grades of polyethylene. However, the averaged percentage variation of failure for the modified Bell Test equaled that of the unaltered Bell Test. As the percentage variance of failure slightly differed between both test methods, this is likely due the limited number of tests conducted, as only one sample was tested at a time. Due to the limited samples tested as well as the differences in the modified Bell Test set up, lengthier testing times were incurred, leaving for a wider margin of variation.

Consequentially in the previous section, approximately 40 samples were analyzed for failure times as well as notch dilation, thus providing for a baseline for variation expected for failure times as well as notch dilation. However, because the modified Bell Test meets the average variation in failure times seen in the unaltered Bell Test, the analysis

of the IGEPAL Transition Time and the Time of IGEPAL Acceleration was the primary focus of this section and not the failure times. In addition to the percentage variation between both the unaltered Bell Test and the modified Bell Test being of similar values, the second LL 8460.29 sample seen in Figure 4.9b) indicated the same trends as Figure 4.9a) and 4.9c). With the variation of failure times as well as the same trend, the skewed LL 8460.29 sample was kept in the dataset for the analysis of both the IGEPAL Transition Time and Time of IGEPAL Acceleration.

It is noted that the increased failure times were primarily due to the difference in the bend angle of a specimen when mounted in the C-clamp up against the load cell, lowering the applied stresses; our tests with different bend angles to establish the functionality of bromocresol green demonstrated this fact. This highlights the sensitivity of the Bell Test to the bend angle of specimens but since the specimens were still found to fail, the methodology was still considered to be appropriately reflecting the environmental acceleration of ESC otherwise found in the Bell Test.

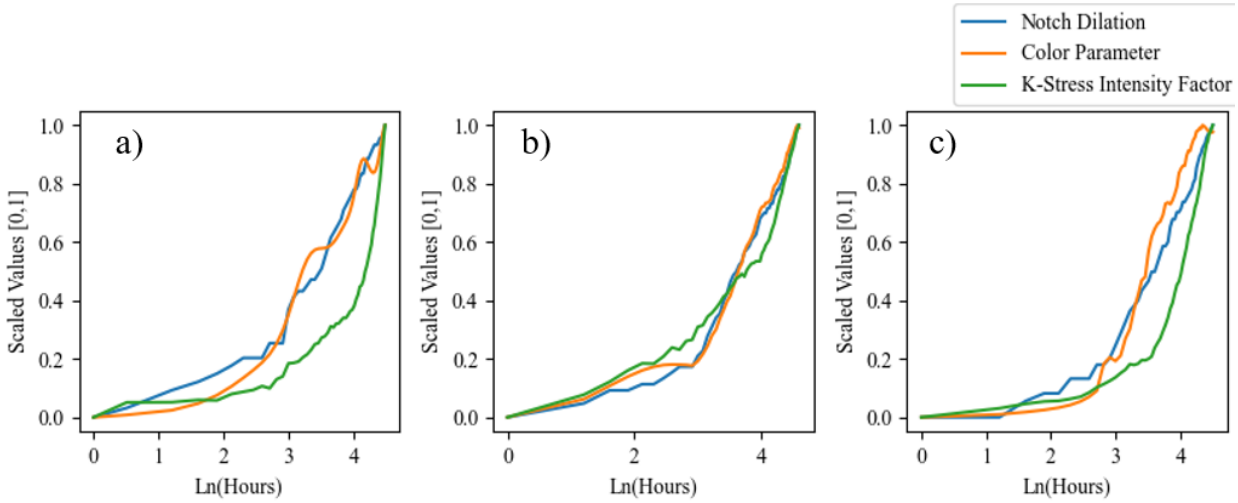

Figure 4.8. Normalized Notch Dilation, Surfactant Concentration (Color Parameter), and stress intensity factor K with respect to time shown for three repeats of HD 8660.29, a) Sample 1, b) Sample 2, c) Sample 3 in the modified test setup

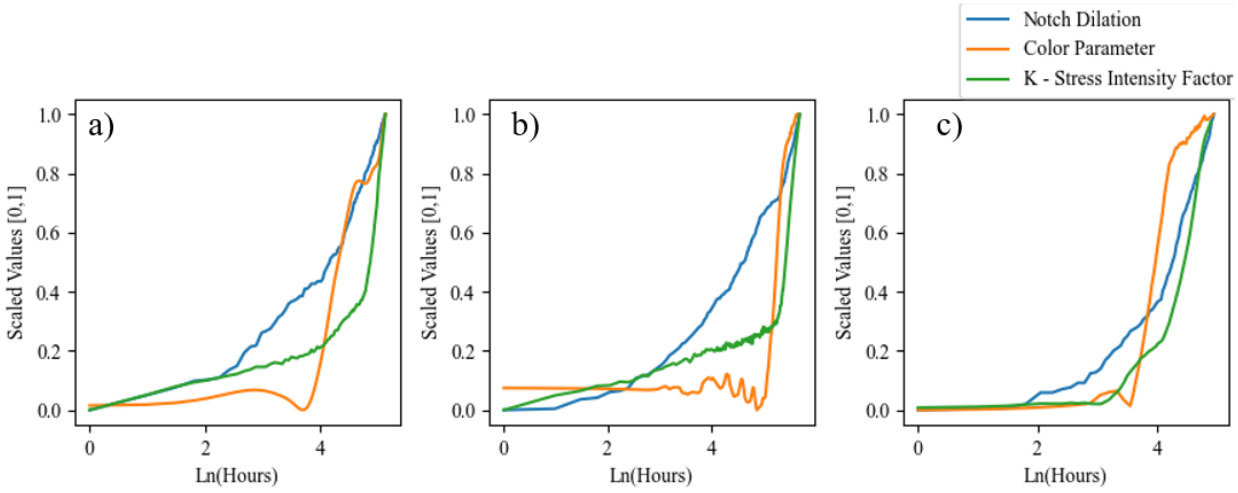

Figure 4.9. Normalized Notch Dilation, Surfactant Concentration (Color Parameter), and stress intensity factor K with respect to time shown for three repeats of LL 8460.29, a) Sample 1, b) Sample 2, c) Sample 3 in the modified test setup

Table 4.3. Transition period highlighted by the IGEPAL Transition Time and Time of IGEPAL acceleration of Notch Dilation, Color Parameter, and Stress Intensity Factor K for two grades of polyethylene

Parameter	**Polyethylene Grade**	**IGEPAL Transition Time (Hours)**	**Time of IGEPAL Acceleration (Hours)**
Notch Dilation	HD 8660.29	16.07 ± 1.95	26.27 ± 15.81
Color Parameter		22.66 ± 13.77	36.06 ± 10.77
Stress Intensity Factor K		27.64 ± 17.65	79.44 ± 11.82
Notch Dilation	LL 8460.29	36.80 ± 11.82	93.11 ± 53.56
Color Parameter		60.18 ± 52.06	114.59 ± 77.65
Stress Intensity Factor K		93.26 ± 25.64	166.29 ± 59.97

The three evaluated elements of ESC relatable to the notch region, namely notch dilation, absorbed surfactant concentration (color parameter), and stress intensity factor K were plotted with respect to time in Figures 4.8 and 4.9, for HD 8660.29 and LL 8460.29 respectively. All three plotted measurements were found to generally increase over the duration of testing, for both polymers, with surfactant concentration showing the greatest variability over time. It is also noted that the trends shown here appeared quite similar to creep behaviour, particularly, the secondary and tertiary phases. Thus, classifying ESC by these unique metrics was seen as complementing current literature on the topic, as will be further explained in the next section. The determined IGEPAL Transition Times and Times of IGEPAL Acceleration for these three qualifiers of ESC are tabulated in Table 4.3 for the two polyethylenes. The data shows a change in the physical state of the polymer was first

occurring by notch dilation followed soon after by the color parameter and finally by stress intensity factor K. This order of transitions was unexpected since it had been originally assumed the concentrated stresses associated with bending were preferentially drawing the surfactant into the notch, with the resulting swelling of the polymer causing cracking and notch dilation. However, in all cases, the transition in stress intensities relating to the bending moment followed the other two factors.

In the two figures, HD 8660.29 was found to show less abrupt changes in the rates of the three plotted measurements before versus after the transition when compared to LL 8460.29; the three measures of ESC for HD 8660.29 samples exhibited a high rate of change in the lag stage and then only modestly increased in rate in the accelerated growth stage whereas for LL 8460.29, these three measures showed relatively little change over time initially but then exhibited a rate even greater than HD 8660.29 after the transition. The results with LL 8460.29 show the subsequent buildup of internal stresses in the part were much more sensitivity to surfactant absorption rather than the size of the notch gap, which is a distinction not so easily seen with HD 8660.29. The phenomena can be attributed to the crystalline structures of the two polymers, with the response of LL 8460.29 reminiscent of strain hardening although now at such a local level that it is difficult to quantify. LLDPE will notably exhibit varied crystalline lamella sizes and lower crystallinity compared to HDPE, on account of impeded crystal growth by its short chain branches [36,37]. The lower crystallinity content of LLDPE (only 44% for LL 8460.29 compared to 50% for HD 8660.29 based on DSC analysis) meant more tie molecules and more chain mobility until highly strained which is likely why all three measures showed

low rates of change before the transition. In comparison, the higher frequency and size of crystals in HDPE meant these hard domains bore much of the deformational strain early in the test leading to stresses concentrating relatively faster in the specimen. Furthermore, the absence of short chain branches in HDPE meant there was less chain hindrance to crystal slip compared to LLDPE [35]. Considering the transition period as a change in the mode of strain deformation where crystal slip becomes increasingly prevalent, then the greater rate in the accelerated growth stage for LL 8460.29 versus HD 8660.29 seems reasonable. Particularly, this is seen with LL 8460.29 which has less crystalline content then HD 8660.29. With less crystalline content present in LL 8460.29, crystal slip showed a higher impact within the acceleration of failure due to limited crystals. Therefore, with limited crystalline content available, crystal slip as well as failure accelerates faster. This can be visually seen in LL 8460.29 Figures 4.9 in comparison to HD 8660.29's Figure 4.8. Consequently, notch areas of failed specimens of HD 8660.29 and LL 8460.29 contained lower crystallinity, 48% and 39% respectively (by DSC), marking a decrease of 2% and 5% from start to end of a trial.

The results of the three measured parameters corresponded well with a different analysis of ESC for the Bell Test conducted using active acoustic spectroscopy to monitor the internal stresses of the HD 8660.29 and LA 080 [7] . In that work it was shown lower crystalline content increased a test specimen's sensitivity to internal stresses (not solely attributed to bending stresses) [7]. Comparatively, in this case the higher crystallinity polyethylene grade and the lower crystallinity polyethylene grade was HD 8660.29 and LA 080; LA 080 displayed a crystallinity content of 61% in that study. As a result of the

previously mentioned sensitivity, lowered crystalline content were noted to show increased moments of changing stresses. This sensitivity was attributed to microstructural asymmetries created by biodiesel penetrating the polyethylene samples [7]. This feature was prevalently seen in LL 8460.29, where LL 8460.29 saw a rapid increase in all metrics previously mentioned.

4.3.3 Proposed additions to the environmental stress cracking mechanism

To explain the development of internal stresses in polyethylene during the Bell Test being monitored by ultrasonic spectroscopy [7], our attention was drawn to the theory of Tonyali et al. [6]. In that earlier study of ESCR, the planar acoustic signal suggested biodiesel exhibited a similar concentration-limited plasticization effect on the polymer, just as Tonyali's theory surmised for IGEPAL CO-630 [6,7]. Both papers are seen as being complimented by the locally notch-specific focus in the present work and its information collected on bending stresses, notch dilation, and absorbed surfactant concentration. Findings in Section 4.3.2.2 are added to the proposed mechanism of Tonyali [6] and its modifications [6,7], in Figure 4.10 shown as a four-step sequence.

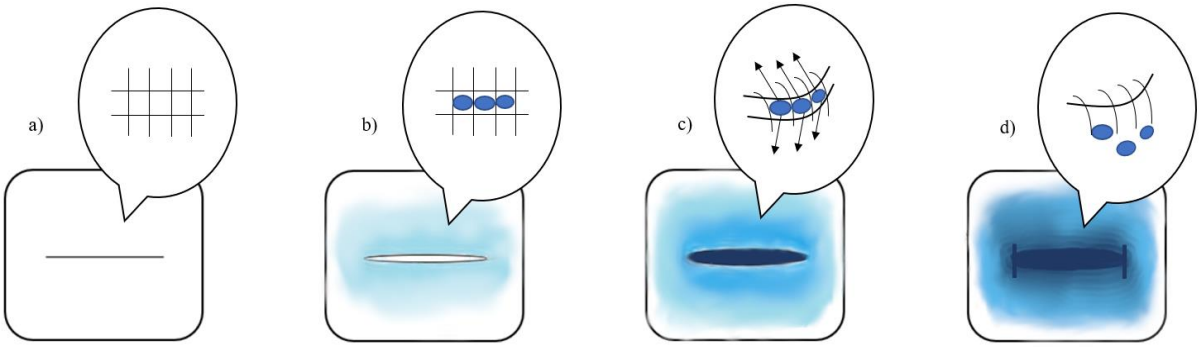

Figure 4.10. Proposed ESC mechanism over time a) Initial bent specimen, b) Initial plasticization indicative of Bromocresol Green's blue staining, indicates that micelles absorbed in between crystalline structures, c) Critical plasticization state, indicating warpage and stress due to the enhanced absorption of IGEPAL CO-630 as well as increased coloring, d) final failure, where crystalline structures can no long hold the definitive structure together.

a) The initial state of the sample contains fibrillated mass generated within its notch due to bending. Since this sample is bent but not yet submerged within the stress cracking agent, internal stresses along the notched area become concentrated (notably at its two apexes) due to the constant external force required to keep the sample bent [6,7]. However, this stage is not the focus of the work presented here and is included as a reference state for the proposed mechanism. Once the bent sample is immersed into the stress cracking agent and some time has passed, an initial plasticization state should occur.

b) During this stage, IGEPAL micelles containing Bromocresol Green causes an initial permanent color change to the polymer due to the preferential absorption of IGEPAL into the highly stressed regions. The observation by the dye corroborated the findings of others that a polymer under stress, such as bending stress at the

notch, will experience concentrated penetration of surface active fluids as well as swelling within these affected regions [38]. The steady increase in notch dilation during the lag stage exposed more areas for the ingress of the stress cracking agent. During this lag stage, acoustic spectroscopy had previously found with biodiesel that the absorbed stress cracking agent causes internal stresses to temporarily decrease in the material [7], even though the load cell in our study showed that bending stresses were only increasing (or stagnant as seen in some cases for HD 8660.29 and LL 8460.29). The lowered internal stresses associated with the surfactant-swollen amorphous regions has been theorized to be caused by interlamellar linkages (primarily cilia) being allowed to stretch more freely [39]. At the same time, stresses measured by the load cell increased due to swelling of the amorphous phase.

c) The IGEPAL Transition Time for stress intensity factor K closely relates to the Time of IGEPAL Acceleration for notch dilation. These two overlapping points are demonstrative of the crystalline structure present whereby tie molecules are trying to contain the expanded amorphous regions caused by plasticization. This state can be called the *plasticization threshold*. With the crystalline structure unable to contain its integrity along the initial defect, a rapid increase in plasticization is noted for IGEPAL which is swelling the amorphous areas at the Time of IGEPAL Acceleration for the color parameter. At this point, the notch and its outer proximate surfaces show a deep blue coloring. With the increased absorption of IGEPAL CO-630 noted by the color parameter's Time of IGEPAL Acceleration, the Time of

IGEPAL Acceleration for stress intensities occurred shortly after. Although, solvent-like plasticization should result in a decline of stresses, the inverse occurs. This is stated due to the bulk measurement of the bending moment for the specimen, where the swelling mentioned causes the ends of the specimen to push outwards against the load cell in the C-clamp. Inherently, this can be seen as an increase in the flexural stresses [40], while the expansion of the notch is a result of increased tensile stresses applied to the notch when compared to its original state. Internally, this swelling due to the surfactant expands the amorphous regions, and further pushes and stretches the crystalline regions, thus causing an increase in internal stresses. Consequentially, the increased swelling as well as the moments leading up to failure were highlighted by Saad et Al's work as a building up of internal stress seen via acoustic analysis [7] . In addition to the bulk measurement of the bending moment of the sample, localized plasticization-like effects directly correspond to expansion in the notch. Additionally, this resultant expansion due to swelling is shown to increase the bending. Throughout testing, a steady amount of lamellar stack rotations occurred in stressed crystalline structures which allowed for a steady conversion of orthorhombic crystals to monoclinic crystals [41]. This can be highlighted by the consistent build up in K-stress intensities shown in Figure 4.8.

d) Once the Time of IGEPAL Acceleration occurred for stress intensities, tie molecules should have disentangled and become stretched with rising internal stresses and a corresponding acceleration in stress intensity factor K is seen [39]. Once this point is reached, micro-voids are visible due to the increased notch

dilation, as the expansion of the entire notch causes the expansion of the micro voids. The physical relationship between the two entities was noted by failed specimens and can be seen in Figure 4.3 (d and e), where blue staining perpendicular to the increasingly dilated notch expanded. These newly formed micro-voids experience steps b and c like the main notch, and further increase in size in both the longitudinal and transverse direction [7]. Consequently, crack propagation is evident and residual failure starts to occur. This crack propagation was highlighted by staining, like the initial staining seen in the notch, making the deep blue area appear to grow and radiate away from the notch.

With respect to the effect of structure of polyethylene (and its related phase morphology) on this mechanism, it has been found in other studies that polyethylenes with a higher degree of short chain branching experience a higher activation energy for ESC [20]; in the present case, LL 8460.29 appears to demonstrate this higher activation energy, shown by all three monitored parameters, comparison to HD 8660.29. We attribute this behavior now to a more tortuous path for IGEPAL absorption being present in LLDPE, stated based on our results showing that fluid absorption preceded stress development in the ESC mechanism. A greater tortuous path for LLDPE compared to HDPE materials has been mentioned in the past for unrelated studies on geomembrane which was looking at absorption profiles of n-alkanes and organic liquids [41,42]. Such a tortuous path would explain the increased time required for the plasticization *threshold* to occur; samples of LL 8460.29 were shown to spend a longer time in stages b and c, and a shortened period of stage d in our study compared to those of HD 8660.29. From the bulk perspective, the key

difference between HD 8660.29 and LL 8460.29 was that LL 8460.29 contains less crystallinity content (due to its short branches content [35]) but this is a minor difference in content and unlikely the primary reason for such a dramatic difference in surfactant absorption, especially since greater amorphous content should aid fluid penetration, rather than hinder. Considering the crystalline morphology of the two polymers, HDPE has a crystalline morphology based on a row nucleated crystal structure consisting of neatly stacked and thick lamellas [43–47] whereas, LLDPE contains thinner, wider, and curvier lamellas [43,45,48,49] and any spherulitic structures of LLDPE tend to be less ordered and more varied in size compared to HDPE [43]. We believe the greater tortuous path created by LLDPE lies in how its crystals are interconnected. As IGEPAL CO-630 absorbed into the amorphous contents of either polyethylene, the swollen amorphous regions increased interlamellar shear and promoted increased crystal slippage [24,43,45,48,49]. The resistance to interlamellar shear for LLDPE corresponded to its increased number of tie molecules available [24]. Comparatively, HDPE contained less tie molecules then LLDPE [50], which allowed for HDPE's crystals to readily move away from the swollen amorphous phase, promoting a path for IGEPAL's ingress relative to LLDPE.

4.4 Conclusion

Exploration of the stress cracking fluid-notch boundary via visualization, displacement and load measurements has provided more details on how ESC progresses. The bromocresol green dye has shown itself as a novel visualization aid in tracking IGEPAL CO-630 sorption within accelerated ESCR testing by its incorporation into

micelles within the stress cracking fluid. By its presence, surfactant absorption was directly monitored as the stress concentrating notch in polyethylene specimens. Simultaneous analysis of surfactant absorption, stress development and notch expansion, the relationship of each over time as the polymer progressively fails in the Bell Test was better understood. Most valuable by this local analysis was the understanding gained on how crystallinity and its association with tie molecules delays the onset of a *plasticization threshold* beyond which absorption of IGEPAL CO-630 leads to an accelerated increase in the K-stress intensity factors as well as notch dilation.

Acknowledgements

The authors would like to thank Imperial Oil Ltd. for their funding of this work. The authors would like to especially thank Ron Cooke at Imperial Oil for his advice, supply of materials, and technical discussions throughout the exploration of the stress cracking fluid-polyethylene boundary within the Bell-Test. We would further like to thank Heera Marway at the McMaster Manufacturing Research Institute (MMRI) for assisting with the development of the load cell set-up of the Bell Test, and finally Hassan Abdulhussain and Austin Bedrosian at McMaster University for their helpful insights in producing the figures shown in the work.

References

[1] M. Schilling, Environmental Stress Cracking (ESC) and Slow Crack Growth (SCG) of PE-HD induced by external fluids, (2019).

[2] D. Wright, Environmental Stress Cracking of Plastics, 1st ed., Rapra Technology Limited, 1996.

[3] K. Tonyali, H.R. Brown, On the applicability of linear elastic fracture mechanics to environmental stress cracking of low-density polyethylene, J Mater Sci. 21 (1986) 3116–3124. https://doi.org/10.1007/BF00553345.

[4] M. Rink, R. Frassine, P. Mariani, G. Carianni, Effects of detergent on crack initiation and propagation in polyethylenes, Elsevier Masson SAS, 2003. https://doi.org/10.1016/S1566-1369(03)80087-0.

[5] P. Chang, J.A. Donovan, Detergent assisted stress cracking in low density polyethylene, Polym Eng Sci. 30 (1990) 1431–1441. https://doi.org/10.1002/pen.760302204.

[6] K. Tonyali, C.E. Rogers, Stress-Cracking of Polyethylene in organic liquids, Polymer (Guildf). 28 (1987) 1472–1477.

[7] A.K. Saad, H.A. Abdulhussain, F.P.C. Gomes, J. Vlachopoulos, M.R. Thompson, Studying the mechanism of biodiesel acting as an environmental stress cracking agent with polyethylenes, Polymer (Guildf). 191 (2020) 122278. https://doi.org/10.1016/j.polymer.2020.122278.

[8] P.D. Frayer, P.P. Tong, W.W. Dreher, The role of intercrystalline links in the environmental stress cracking of high density polyethylene, Polym Eng Sci. 17 (1977) 27–31. https://doi.org/10.1002/pen.760170105.

[9] X. Lu, N. Brown, Effect of thermal history on the initiation of slow crack growth in linear polyethylene, Polymer (Guildf). 28 (1987) 1505–1511. https://doi.org/10.1016/0032-3861(87)90350-8.

[10] M.E.R. Shanahan, The role of the liquid in environmental stress cracking of polyethylene, J Mater Sci Lett. 2 (1983) 28–32. https://doi.org/10.1007/BF00719949.

[11] M.E.R. Shanahan, J. Schultz, The Influence of Spherulitic Size on the Environmental Stress Cracking of Low Density Polyethylene, 1126 (1980) 1121–1126.

[12] J. Cazenave, B. Sixou, R. Seguela, Structural Approaches of Polyethylene Environmental Stress-Crack Resistance, Oil & Gas Science and Technology. 61 (2006) 735–742. https://doi.org/10.2516/ogst.

[13] M. Razavi-Nouri, J.N. Hay, Thermal and dynamic mechanical properties of metallocene polyethylene, J Appl Polym Sci. 42 (2001) 8621–8627. https://doi.org/10.1002/app.1988.070350710.

[14] L. D'Agnillo, J.B.P. Soares, A. Penlidis, Controlling molecular weight distributions of polyethylene by combining soluble metallocene/MAO catalysts, J Polym Sci A Polym Chem. 36 (1998) 831–840. https://doi.org/10.1002/(SICI)1099-0518(19980415)36:5<831::AID-POLA16>3.0.CO;2-H.

[15] Byoung-Ho Choi, Weinhold Jeffrey, Reuschle David, Kapur Mridula, Modeling of the Fracture Mechanism of HDPE Subjected to Environmental Stress Crack Resisttance Test, Polym Eng Sci. (2009) 2085–2091. https://doi.org/10.1002/pen.

[16] M. Demirors, The History of Polyethylene, 2011. https://doi.org/10.1007/978-1-4614-6504-1_1.

[17] P. Sardashti, K.M.E. Stewart, M. Polak, C. Tzoganakis, A. Penlidis, Operational maps between molecular properties and environmental stress cracking resistance, J Appl Polym Sci. 136 (2019) 1–10. https://doi.org/10.1002/app.47006.

[18] K. Tribe, G. Saunders, R. Meißner, Characterization of branched polyolefins by high temperature GPC utilizing function specific detectors, Macromol Symp. 236 (2006) 228–234. https://doi.org/10.1002/masy.200690059.

[19] R.A. Bubeck, H.M. Baker, The influence of branch length on the deformation and microstructure of polyethylene, Polymer (Guildf). 23 (1982) 1680–1684. https://doi.org/10.1016/0032-3861(82)90193-8.

[20] J.J. Cheng, M.A. Polak, A. Penlidis, Influence of micromolecular structure on environmental stress cracking resistance of high density polyethylene, Tunnelling and Underground Space Technology. 26 (2011) 582–593. https://doi.org/10.1016/j.tust.2011.02.003.

[21] P.M. Wood-Adams, The effect of long chain branches on the shear flow behavior of polyethylene, J Rheol (N Y N Y). 45 (2001) 203–210. https://doi.org/10.1122/1.1332785.

[22] J.J. Cheng, M.A. Polak, A. Penlidis, Polymer network mobility and environmental stress cracking resistance of high density polyethylene, Polymer - Plastics Technology and Engineering. 48 (2009) 1252–1261. https://doi.org/10.1080/03602550903159085.

[23] J.J. Cheng, M.A. Polak, A. Penlidis, A tensile strain hardening test indicator of environmental stress cracking resistance, Journal of Macromolecular Science, Part A: Pure and Applied Chemistry. 45 (2008) 599–611. https://doi.org/10.1080/10601320802168728.

[24] J.J. Cheng, M.A. Polak, A. Penlidis, Phase interconnectivity and environmental stress cracking resistance of polyethylene: A crystalline phase investigation, Journal of Macromolecular Science, Part A: Pure and Applied Chemistry. 46 (2009) 572–583. https://doi.org/10.1080/10601320902851801.

[25] A.K. Saad, F.P.C. Gomes, M.R. Thompson, Plasticizing effect of oxidized biodiesel on polyethylene observed by nondestructive method, Fuel. 252 (2019) 246–253. https://doi.org/10.1016/j.fuel.2019.04.122.

[26] H.R. Brown, A theory of the environmental stress cracking of polyethylene, Polymer (Guildf). 19 (1978) 1186–1188. https://doi.org/10.1016/0032-3861(78)90069-1.

[27] S. Bandyopadhyay, H.R. Brown, Studies of Environmental Stress-Crack Propagation in Low-Density Polyethylene., Journal of Polymer Science. Part A-2, Polymer Physics. 19 (1981) 749–761. https://doi.org/10.1002/pol.1981.180190504.

[28] ASTM International, Standard Practice for Compression Molding Thermoplastic Materials into Test Specimens, Plaques, or Sheets, (2016) 1–13. https://doi.org/10.1520/D4703-16.2.

[29] ASTM, ASTM D1693.15 - Standard Test Method for Environmental Stress-Cracking of Ethylene Plastics, ASTM International. (2015) 1–11. https://doi.org/10.1520/D1693-15.2.

[30] A.L. Ward, X. Lu, Y. Huang, N. Brown, The mechanism of slow crack growth in polyethylene by an environmental stress cracking agent, Polymer (Guildf). 32 (1991) 2172–2178. https://doi.org/10.1016/0032-3861(91)90043-I.

[31] H. Tada, P.C. Paris, G.R. Irwin, Stress Analysis Results for Common Test Specimen Configurations, The Stress Analysis of Cracks Handbook, Third Edition. (2010) 39–80. https://doi.org/10.1115/1.801535.ch2.

[32] A.R. Petcu, E.A. Rogozea, C.A. Lazar, N.L. Olteanu, A. Meghea, M. Mihaly, Specific interactions within micelle microenvironment in different charged dye/surfactant systems, Arabian Journal of Chemistry. 9 (2016) 9–17. https://doi.org/10.1016/j.arabjc.2015.09.009.

[33] J.N. Robinson, A.S. Tetelman, The relationship between crack tip opening displacement, local strain and specimen geometry, Int J Fract. 11 (1975) 453–468. https://doi.org/10.1007/BF00033532.

[34] M. Thuy, M. Pedragosa-rinc, U. Niebergall, H. Oehler, I. Alig, M. Böhning, Environmental Stress Cracking of High-Density Polyethylene Applying Linear Elastic Fracture Mechanics, (2022).

[35] J.T. Yeh, J. -H Chen, H. -S Hong, Environmental stress cracking behavior of short-chain branch polyethylenes in Igepal solution under a constant load, J Appl Polym Sci. 54 (1994) 2171–2186. https://doi.org/10.1002/app.1994.070541320.

[36] X. Lu, R. Qian, N. Brown, The effect of crystallinity on fracture and yielding of polyethylenes, Polymer (Guildf). 36 (1995) 4239–4244. https://doi.org/10.1016/0032-3861(95)92219-5.

[37] S. Hosoda, H. Nomura, Y. Gotoh, H. Kihara, Degree of branch inclusion into the lamellar crystal for various ethylene/α-olefin copolymers, 31 (1999) 1999–2005.

[38] P. Hittmair, R. Ullman, Environmental stress cracking of polyethylene, J Appl Polym Sci. 6 (1962) 1–14. https://doi.org/10.1002/app.1962.070061901.

[39] A. Lustiger, R.L. Markham, Importance of tie molecules in preventing polyethylene fracture under long-term loading conditions, Polymer (Guildf). 24 (1983) 1647–1654. https://doi.org/10.1016/0032-3861(83)90187-8.

[40] C. Bastioli, G. Romano, C. Migliaresi, Water sorption and mechanical properties of dental composites, Biomaterials. 11 (1990) 219–223. https://doi.org/10.1016/0142-9612(90)90159-N.

[41] T.M. Aminabhavi, H.G. Naik, Molecular migration of low sorbing organic liquids into polymeric geomembranes, Polym Int. 48 (1999) 373–381. https://doi.org/10.1002/(SICI)1097-0126(199905)48:5<373::AID-PI149>3.0.CO;2-9.

[42] T.M. Aminabhavi, H.G. Naik, Chemical compatibility of geomembranes - sorption, diffusion and swelling phenomena, Journal of Plastic Film and Sheeting. 15 (1999) 47–56. https://doi.org/10.1177/875608799901500106.

[43] M.F. Butler, A.M. Donald, W. Bras, G.R. Mant, G.E. Derbyshire, A.J. Ryan, A Real-Time Simultaneous Small- and Wide-Angle X-ray scattering Study of In-Site Deformation of Isotropic Polyethylene, Macromolecules. 28 (1995) 6383–6393.

[44] R. Stein, S., Some scattering studies of polymer microstructures, surfacesm and interfaces, Pure and Applied Chemistry. 63 (1991) 941–950. https://doi.org/10.1007/978-3-319-29917-4_8.

[45] H. Sano, T. Usami, H. Nakagawa, Lamellar morphologies of melt-crystallized polyethylene, isotactic polypropylene and ethylene-propylene copolymers by the RuO4 staining technique, Polymer (Guildf). 27 (1986) 1497–1504. https://doi.org/10.1016/0032-3861(86)90094-7.

[46] X.M. Zhang, S. Elkoun, A. Ajji, M.A. Huneault, Oriented structure and anisotropy properties of polymer blown films: HDPE, LLDPE and LDPE, Polymer (Guildf). 45 (2004) 217–229. https://doi.org/10.1016/j.polymer.2003.10.057.

[47] H. Hajová, R. Pokornaý, J. Kosek, Diffusion transport in reconstructed semi-crystalline structure of polyolefins, Macromol Symp. 302 (2011) 121–128. https://doi.org/10.1002/masy.201000073.

[48] S. Hosoda, K. Kojima, M. Furuta, Morphological study of melt-crystallized linear low-density polyethylene by transmission electron microscopy, Die Makromolekulare Chemie. 187 (1986) 1501–1514. http://onlinelibrary.wiley.com/doi/10.1002/macp.1986.021870619/abstract.

[49] P.P. Kundu, J. Biswas, H. Kim, S. Choe, Influence of film preparation procedures on the crystallinity, morphology and mechanical properties of LLDPE films, Eur Polym J. 39 (2003) 1585–1593. https://doi.org/10.1016/S0014-3057(03)00056-9.

[50] M.F. Butler, A.M. Donald, Deformation of spherulitic polyethylene thin films, J Mater Sci. 32 (1997) 3675–3685. https://doi.org/10.1023/A:1018642732686.

Chapter 5. Automation of the Bell Test

Automation of ESCR Testing via Computer Vision application toward the Bell Test

V. Gritsichine, J. Vlachopoulos, M. R. Thompson*

CAPPA-D/MMRI, Department of Chemical Engineering,

McMaster University, Hamilton, Ontario, Canada

Abstract

This chapter outlines the development of a machine-learning directed visual analysis system for automating a standardized test for environmental stress cracking resistance among polymer grades with the purposes of improving its repeatability. The proposed method applies three convolutional neural networks to identify specimens in video-recorded images, classify the failed specimens in an isolated test environment, and create a predictive regression for the ever-expanding notch in Bell Test specimens prior to their failure. The computer vision application was deemed to be accurately determining the failure times of polymers, detecting specimen failures in a timely manner when compared to operators, and applying a more consistent criteria for when a specimen had failed. This approach was shown to reduce the historically high variability indicative of the Bell Test.

5.1. INTRODUCTION

Polyethylene is a semi-crystalline polymer with a 31% share of the thermoplastic market and contains a global demand of nearly 154 billion pounds annually [1,2]. The reasons for its popularity include low cost, ease of processing, chemical resistance, toughness, as well as flexibility at low temperatures [2,3]. These factors make this polymer an excellent candidate for packaging, piping, and film applications [2,3]. More than a few of these applications demand prolonged, reliable performance in the presence of potentially damaging factors where part failure is equated with high recovery costs. One unique mode of failure for polyethylene, particularly for its characteristic chemical resistance, is environmental stress cracking (ESC) where long-term exposure of the polymer to specific chemicals can dramatically reduce the service life of parts; ESC accounts for 15% of all known failures for polymer parts [4].

Due to the critical nature of parts in service with a higher likelihood for ESC failure, accelerated testing to detect polymer sensitivity to ESC is very important. The first test and the most widely used test in industrial settings for evaluating environmental stress cracking resistance (ESCR) is the ASTM-D1693 standard, better known as the Bell Test [5]. The Bell Test evaluates a polymer under accelerating conditions, which involves submersing ten bent and notched test specimens in a concentrated or dilute solution of nonylpheoxy poly(ethyleneoxy) ethanol, known as IGEPAL CO-630 [6]. An operator is advised to monitor the test during the 0.1h, 0.25h, 0.5h, 1.0h, 1.5h, 2h, 3h, 4h, 5h, 8h, 16h, 24h, 32h, 40h, and 48h checkpoints as stated by the ASTM standard. Extended tests (tests longer then

48h) are suggested by the ASTM to be checked once a day. Once failures of the specimens are recorded, the ESCR performance of the polymer is characterized by two methods. The classification of failure is based on whether the crack is detected by an operator with "normal eyesight" as stated by the ASTM standard. However, due to the subjectiveness of failure, failure may be apparent to one operator and not the other, thus obstructing failure times used for further classification of ESCR performance. The first ESCR metric is f_{50}, which is the recorded time for when five out of ten specimens have failed. The second method of classifying ESCR performance is based on recording all the samples failure times and producing a line of best fit describing the probability of failure. The line of best fit is used to determine the F_{50} value, which is the probability of when 50% of the samples tested will fail.

Although the Bell Test is a rapid and convenient test in determining ESCR ratings, the Bell Test faces various reproducibility issues such as defining what constitutes a 'failure' as well as the ill-defined inspection times of specimens past the first 48 hours of testing [5]. The f_{50} and F_{50} metrics were derived due to the inability of the operator to be present for every minute of a test; however, resins with good ESCR will show less variability by following the standard as a result since failures will only be assessed every 24 hours in such cases. With these reproducibility issues present in the Bell Test, the f_{50} and the F_{50} value can be skewed as well as inaccurate when assigning ESCR to various polyethylene grades.

Given recent advancements in technology, detecting cracking in materials has been made easier via computer vision as well as artificial intelligence [7–9]. This work

contemplates the possible improvements to the Bell Test when a novel set of convolutional neural network models are applied in order to increase reproducibility and failure detection in the Bell Test.

5.2. EXPERIMENTAL

5.2.1 Set Up

5.2.1.1 Materials

A high-density polyethylene grade (HDPE HD 8660.29) and a linear low density polyethylene grade (LLDPE LL 8460.29) were provided as pellets by Imperial Oil LTD (Sarnia, On). These two grades of polyethylene had relatively low rated environmental stress cracking resistance (F_{50}) and similar melt flow index (MFI) values. Respectfully, HD 8660.29 had a density of 0.941 g/cm^3, 2.0 g/10min MFI, and F_{50} of 40 h, while LL 8460.29 had a density of 0.938 g/cm^3, 3.3 g/10 min MFI, and F_{50} of 60 h. Square plaques of both resins were compression molded following Procedure C in Annex 1 of the ASTM D-4703 [10]. Once the plaques were made, test strips of 38 mm x 13 mm x 3 mm (thickness) were cut from the plaque, in accordance with ASTM-D1693. All test specimens were left to rest for 48 hours before testing.

5.2.1.2 Bell Test

Test specimens were notched by the nicking-jig highlighted in the ASTM D-1693 standard given for the Bell Test. Once the test specimens were notched, specimens were bent over a 30 second period and then transferred into a brass carrier using the transfer tool

specified in the standard [6]. Each carrier contained five specimens (i.e. less than the standard ten so they could be seen simultaneously by a camera) and were immersed in a 75 ml glass test-tube containing a modified stress cracking solution consisting of 10% IGEPAL C0-630 (Sigma Aldrich; Mississauga ON) dissolved in Milli-Q purified water with 0.01 wt% Bromocresol Green dye added as a tracer. Seven test-tubes were tested at the same time, controlled to 50 °C using a circulating water bath. Progress of the test was monitored using an Envenox Web Camera with a 125^{o} viewing angle and 1280 x 720 pixel resolution, mounted in front of the water bath holding the test-tube. The camera was controlled via a Python V3.8 coded script to record an image every 10 minutes. Average failure times for a resin grade were calculated from the recorded images.

5.2.2 Proposed Automated Computer Vision Model

5.2.2.1 Process Flow Chart and Training Details

The computer vision system relied upon supervised convolutional neural network (CNN) models to transpose image information acquired from the Bell Test for up to seven test tubes into a measure of notch expansion and classify samples as either intact or fractured. The developed tool offers an approach to accurately assess environmental stress cracking during the Bell Test based on dimensional analysis of the notch area in each specimen. The sequence of neural network systems can be seen in Figure 5.1.

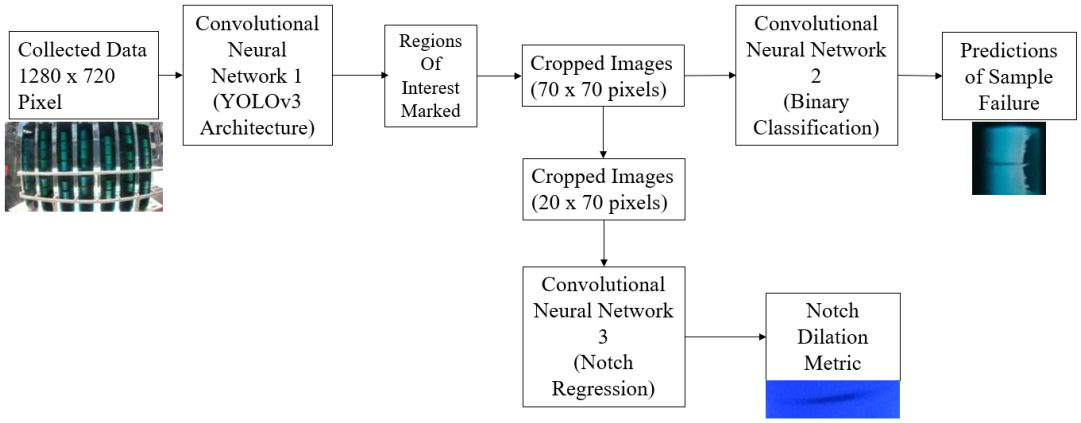

Figure 5.1. Proposed Computer Vision Model for the Bell Test

Training data was created using LabelIMG, a python-based freeware program that allows the regions of interest (ROI) in images previously taken during a test, to be identified for analysis with their text coordinates; there were up to 35 ROI per image to be identified and over time the coordinates changed slightly. These coordinates changed due to the glass tubes containing the Bell Test carriers shifting due to the circulating water bath used to heat the bath up, thus moving the specimen's positions over the duration of testing. A square-outlined 70 x 70 pixel labelled region was appropriate to display the notched end of each bent specimen, which LabelIMG recorded via four descriptors corresponding to the x- and y-coordinates for the bottom left corner, edge width (w), and edge length (l). These labelled sections of an image were used to train the first convolutional neural network. The second CNN model cropped out the labelled sections from the original images for training. These cropped images were designated as 0 if the sample seen in it had not failed, or 1 if there was evidence that a failure occurred. Both the labelled sections of an original image and cropped images were used to train the second convolutional neural network model. The

third CNN model which only needed to focus on the notch opening, further cropped the previously cropped image to 70 x 20 pixels. This refined area gave a better assessment of the notch dimension as it opened using Image-J software (National Institute of Health, USA).

For the training of the *YOLOv3* model, 10,000 images were used for the training data for *YOLOv3*. These images contained 35 bounding boxes per image. Additionally, 2000 images were used for the testing set of *YOLOv3*, making for an 80:20 split of training and testing. Due to the simplicity of the second convolutional neural network, the second convolutional neural network was trained on 5000 images, where half of the images were failed samples and the other half being non-failed samples. The testing set for the second convolutional neural network contained 10,000 images, containing 10 samples of HD 8660.29 and 10 samples of LL 8460.29. The third convolutional neural network was trained on 1000 images containing their respective notch dilation values. The testing set for the third convolutional neural network contained 130 images, providing for a 87:13 training and testing set.

5.2.2.2 Proposed Models Architecture and Metrics

The first CNN model in the system, “You Only Look Once Version 3” (YOLOv3), was used to recognize each test specimen in captured images showing up to 35 specimens being simultaneously tested in the water bath, trained with the labelled images using LabelIMG mentioned above. The neural network was configured with an input layer, 53 predetermined hidden layers, and an output layer detecting the class of item along with the

bounding box coordinates [11]. A custom loss function which was based on minimizing the error in bounding box coordinates with respect to the mean intersection of union was used for training [11].

The second CNN model was used to classify whether a sample had failed or not, based on cropped images of the Bell Test setup monitored by the camera and trained with the cropped images extracted from the captured camera view. The sequence of layers for the second CNN consisted of an input layer handling the three-layered images, one convolutional based hidden layer, one user defined filter, one convolutional based hidden layer, one user defined filter, and one convolutional based hidden layer. The two user defined filters adjusted the image from the convolutional based hidden layer by sampling 3 x 3 areas within the photo and replaced the entirety of the 3 x 3 area with the darkest pixel (each pixel in the 3x3 area). The refined view in these images was used to focus on the notch and any perpendicular cracking, which displayed as darker pixels. Once the image data was passed through the previously mentioned layers and filters, it was flattened into a one-dimensional row and fed into another hidden layer consisting of 128 weights and biases, commonly referred to as nodes. Once passed through the last hidden layer, the predictions of whether a sample has failed or not were outputted by the output layer as a binary solution. All hidden layers for the second CNN used rectified linear unit functions as activation functions, while the output layer consisted of a sigmoid activation function. The binary cross entropy loss function was used to train the second CNN model, while the accuracy metric was used to measure the performance of the second CNN model on the testing data. Both equations can be seen in Equations (5.1) and (5.2). Once the model was

trained, predictions of the model were fitted by a sigmoid function via SciPy's Curve Fit function within Python. This was done to produce a failure time encompassing the initial sighting of a micro void. The sigmoid function can be seen in Equation (5.3)

The third and final CNN model identifies the edges of the notch in order to estimate its expansion over time, referred to as notch dilation. This model accepted the same cropped images used by the second CNN model. The structure of the third CNN model consisted of an input layer, one hidden convolutional layer, one user defined filter, a flattening layer, and a cascade of five hidden layers consisting of 256, 128, 64, 32, 16 nodes. After the last hidden layer, an output layer consisting of a linear activation function was used to produce predictions of the edge-to-edge distance of the notch transverse to its longitudinal length. The user defined filter is the same filter used in the second CNN model; however, a 9 x 9 area was used instead of a 3 x 3 area to replace the darkest pixel within the selected area. Subsequentially, the loss function used for training was the root mean squared function, and the metric used during training and testing to compare, monitor, and measure performance during training was the mean average error. Both equations can be seen in Equations (5.4) and (5.5). Once the notch measurements were produced, a Logistic Growth function was regressed to describe the trajectory of the notch dilation metric, which can be seen in Equation (5.6). The performance of the third CNN model was compared to manually measured notch dilation of the testing set. Both the second and third CNN models were implemented by using the TensorFlow 2.6 library native to Python.

$$Binary\ Cross\ Entropy = \frac{1}{N}\sum_{i=1}^{N} y_i \times Log\left(y_{predicted}\right) + \left(1 - y_{true}\right) \times \log\left(1 - y_{predicted}\right) \quad (5.1)$$

$$Accuracy\ Metric = \frac{Total\ Correct\ Predictions}{Total\ Number\ of\ Predictions} \quad (5.2)$$

$$Sigmoid = \frac{1}{1+e^{-x}} \quad (5.3)$$

$$Root\ Mean\ Square\ Error\ (RMSE)\ = \sqrt{\frac{\sum_{i=1}^{N}\left(y_{true} - y_{predicted}\right)^2}{N}} \quad (5.4)$$

$$Mean\ Absolute\ Error\ (MAE) = \frac{\sum_{i=1}^{n}|y_{predicted} - y_{true}|}{n} \quad (5.5)$$

Logistic Growth Function $Notch\ Dilation\ (mm) = \frac{a}{1+b(e^{-cx})}$ (5.6)

5.3. RESULTS AND DISCUSSION

5.3.1 Overall Performance of the Model

5.3.1.1 Evaluation of the application of Convolutional Neural Networks for the Regression of Notch Dilation

A key indicator described in Chapter 4 suggests that expansion of the notch (referred to as notch dilation) may be able to forewarn of imminent failure by ESC before fracturing occurs, which allow operators to make an informed decision whether a very long test should continue by the knowledge that it will eventually break. This is done by determining the time of which acceleration occurs, as it corresponds with the transition of the increased stress intensities seen in Chapter 4. Given that this descriptor of ESC can be automated by the third CNN model, it was included in the proposed on-line monitoring system. Considering, the computational demands of the third CNN model, as well as fluctuating lighting conditions throughout testing that affects notch visibility, only one specimen in a specific location within the camera's viewpoint was focused on throughout

the duration of testing (though the system can identify up to 35 specimens simultaneously). The notch measurements were done on images collected every 30 minutes apart from one another. This specimen of interest was picked by the operator before testing began to ensure it was being tracked under optimal lighting conditions. Previous trials indicated that specimens with optimal lighting conditions generally were in the center of the water bath. Particularly, this was evident as samples towards the ends of the water bath garnered less light, making a notch less visible. The notch dilation monitoring system was tested on data the model had never seen before and compared to operator's measurements. For the presented test case in this work, the notch dilation's convolutional neural network was used to observe a sample of LL 8460.29. The operators' measurements for this test set were treated as the control for what the CNN should optimally achieve, with data shown in Figure 5.1. Initial results from the CNN model used to determine the notch dilation values suggest that the developed CNN for the determination of the notch dilation measurements can be successfully used if fine tuned more.

The need for improvement stems from the variance between images analyzed by the convolutional neural network. Inherently, this can be attributed to the lighting conditions mentioned earlier, where the notch dilations convolutional neural network produced results that varied as time progressed, cycling based on the natural lighting since the test setup was partially illuminated by external lighting conditions. Besides additional training and testing that can be conducted on the notch dilations convolutional neural network, a pre-processing filter may be capable of standardizing images to reflect a singular lighting condition. Additionally, it is seen that after the 35 hour mark of testing, the notch

dilations convolutional neural network produced results consistently lower then the operators measurements. This is attributed to less training data being available for highly dilated notches since often the test specimens had completely failed before this point in time. Particularly, when a test has failed, the test tubes are generally taken out and the recording of the test stops. With limited amounts of data relating to highly dilated notches, the notch dilations convolutional neural network produces values slightly below higher dilated notch values. To improve this model, larger amounts of data containing higher notch dilation values past failure can be included

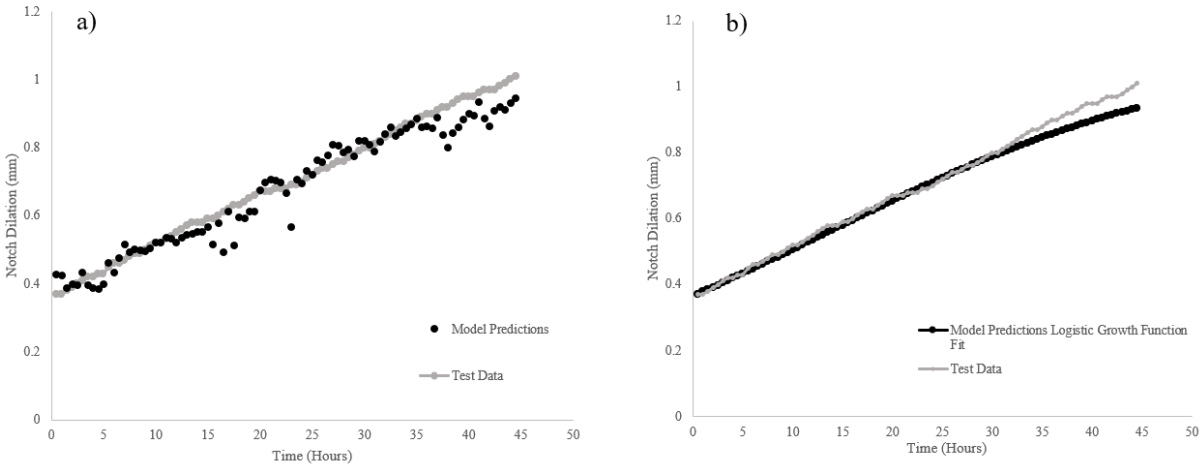

Figure 5.1. Notch Dilation a) Test Data and CNN predicted values (RMSE=0.045, MAE=0.0346), b) Test Data fitted to a Logistic Growth Function (RMSE =0.035, MAE=0.0192)

Interpreting the trend for notch dilation in the presence of the variance mentioned by lighting, was improved with fitting of a logistic growth function, seen in Figure 5.1b; a lowered RMSE and MAE value is reported with use of the function. This approach was

hoped to speed up the training of the CNN model though it appears to under-predict notch dilation at high test times and this is not due to the training deficiencies seen with the CNN model. And so, the function might have uses for interpreting physical phenomena in the data but not to aid the CNN model's training.

5.3.1.2 Evaluation of the application of YOLOv3 and the Classification Model

The Bell Test is essentially a classification technique based on visual data assessed over a prolonged period, making its automation feasible with new machine learning techniques. The *"You Only Look Once Version 3"* model was pivotal to this automation since each test involved up to 35 specimens being recorded from over 500 images, offering a high amount of data for the two subsequent CNN models. YOLOv3 was found to accurately provide bounding boxes for all 35 bent specimens in the testing apparatus with ~98% accuracy. The reason for using YOLOv3 for determining where the bounding boxes of the sample is that over time the Bell Test carrier would shift from its original location, causing the specimens to change position with respect to the camera's field of view. Consequentially, manually cropping the specimens within the image would require extraneous efforts.

With all individual specimens identified in the collected images for a test, the second CNN model reported an accuracy by Equation (5.2) of 93% in detecting unbroken specimens and 96% accuracy for fractured specimens deemed to have failed for a labelled testing set. The result of the second CNN model can be improved by using additional data for training and validating as well as tuning the neural network further. An example of the

subtle differences in the captured images being correctly classified by the model, is seen in Figure 5.2 for HD 8660.29.

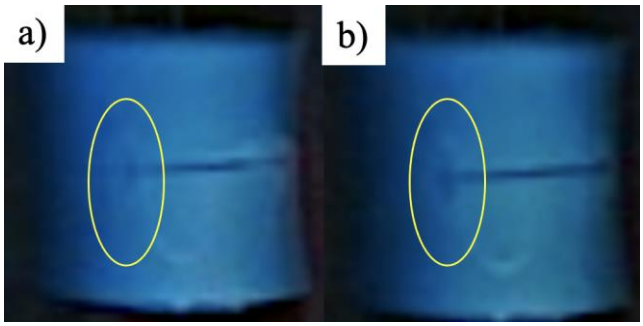

Figure 5.2. Comparison of failures highlighted in yellow a) Second CNN model Prediction (44.16 hours), b) Confirmed Failure by an operator (47 hours)

The second CNN model addresses the concerns of subjectiveness in what constitutes a failure by accurately determining the first appearance of a micro void, which may occur between 5-15 hours earlier than complete specimen failure. Admittedly, the second CNN model was trained by a single operator's definition of a failure and that may need more operators' input to finalize this model for broader use. By providing a concrete definition of what failure is, the second CNN model can predict, confirm, and recognize the initial sighting of the micro-void, thus being on par with the operator. Further discussions about the performance and comparison between the operator and the second CNN model can be seen in Section 5.3.2.

The second CNN model relied upon the Bromocresol Green dye to better distinguish micro voids when compared to the standard 10% IGEPAL CO-630 solution. As seen in Chapter 4, bromocresol green will highlight a notched area, as well as provide a visual aid for the absorption of IGEPAL CO-630 into this defect. A comparison of fully

failed specimens of HD 8660.29 can be seen in Figure 5.3. With the inclusion of Bromocresol Green additive, fracturing of polyethylene samples was increasingly easier to see, aiding in the detection of micro-voids as early as possible.

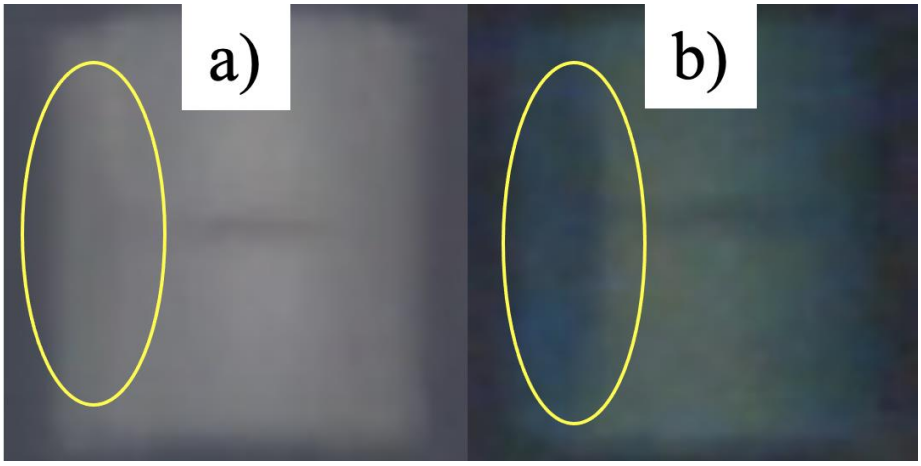

Figure 5.3. Fully failed HD 8660.29 samples a) HD 8660.29 submerged in a 10% IGEPAL CO-630 solution b) HD 8660.29 submerged in a 10% IGEPAL CO-630 solution + 0.01wt% Bromocresol Green

5.3.2 General Discussion

It was seen by the classification of failures that the proposed computer vision system for tracking an on-going Bell Test can be on par with one manned by an operator. A comparison between the F_{50}, f_{50}, averaged operators' failure time of each specimen, and the predicted failure times done by the second convolutional neural network can be seen in Table 5.1. It is shown in Table 5.1 that all the failure times share similar values, which is an indication that the second convolutional neural network produced reasonable predictions of failure. However, one key difference between the determination of the F_{50} and f_{50} values

in Table 5.1 is that the ability to assess failure from more frequent observations of the test system provides for increased accuracy; a human operator could achieve the same accuracy but would need to continuously watch the specimens, which is not feasible and neglects the likelihood that fatigue will harm the operator's judgement.

It was shown through Table 5.1, that the F_{50} times recorded in the technical data sheets as well as the f_{50} and F_{50} values calculated in this study for both grades of polyethylene fell in the standard deviations for both the average failure time calculated by the operator and the predicted failure time calculated by the classification convolutional neural network. However, given the increased standard deviations for the predicted failure times, the F_{50} failure times recorded in the technical data sheets are closer to the both ends of the standard deviation within the predicted failure times calculated by the classification convolutional neural network model when compared to the average failure times calculated by the operator. This can be justified as a positive outcome as it indicates that the binary classification model contains higher confidence in predicting the true failure time when compared to the standard deviations determined by the average failure time. This is also an indication that the second convolutional neural network was not overfit towards the operator's definition of what a failure is. The original method of determining both the F_{50} and f_{50} values can be seen in Tables 5.2 and 5.3.

Table 5.1. Failure time comparison for F_{50}, f_{50}, Averaged failure specimen time, predicted failure time

Polyethylene Grade	F_{50} Failure Time (Hours)	f_{50} Failure Time (Hours)	Average Failure Time Calculated by Operator (Hours)	Predicted Failure Time Calculated by Classification Convolutional Neural Net Work (Hours)
HD 8660.29	51.13	50.33	52.16 ± 7.0	54.71 ± 10.99
LL 8460.29	52.10	52.83	53.21 ± 7.0	55.43 ± 8.06

Tables 5.2 and 5.3 demonstrated that with a 24 hour interval for checking the state of specimens, as indicated in the ASTM-1693 standard for resins with ESCR testing times longer then 48 hours, both the F_{50} and f_{50} failure times become heavily skewed towards larger values. The failure times are reportedly shorter with more frequent observations of specimens in the Bell Test. Since the polyethylene grades tested in this work had F_{50} values on the lower bounds of starting to check every 24 hours, the relative error in detecting a failure is greater than for grades with ESCR of hundreds of hours. An example of this is if a sample fails at the 41^{st} hour of the test, the recorded failure time will be 48 hours, representing a 17% error and in the 49^{th} hour, the recorded failure time will be 72 hours resulting in a 49% error. These errors additionally apply to both the F_{50} and f_{50} values. Conversely, in the case of higher ESCR rated polyethylene grades, such as HD 9830.02 (F_{50}~370 hour), a failure at 394 hours will be recorded at 408 hours resulting in a 3.5% error.

Table 5.2. F_{50} determination via 6, 12, 24-hour checks

Polyethylene Grade	**6 hours check point (h)**	**12 hours check point (h)**	**24 hours check point (h)**
HD 8660.29	53.39	56.17	60.67
LL 8460.29	53.96	56.45	62.37

Table 5.3. f_{50} determination via 3, 6, 12, 24-hour checks

Polyethylene Grade	**6 hours check point (h)**	**12 hours check point (h)**	**24 hours check point (h)**
HD 8660.29	54	60	72
LL 8460.29	54	60	72

Based on this analysis of how the frequency of checking specimens for failure can impact the determination of ESCR ratings like F_{50} and f_{50}, a feasible approach to continuously monitoring to be appropriate to lowering the variability in ESCR assessments. Since the performance of the CNN model similarly matches the performance of an operator (and may be more sensitive to microvoids) and continuously monitors, this new approach is considered an improvement to the Bell Test.

5.4. CONCLUSION

The automation of the Bell Test via computer vision was shown possible by the application of a series of convolutional neural networks. It was shown that the series of convolutional neural networks performed well on data it has never seen before, and therefore can be used as a real-time monitoring system. The series of convolutional neural networks at this stage of development, however, was shown to be used as a labour-saving tool, as it can analyze the Bell Test after completion. Both positive outcomes, rely on the basis of moving the Bell Test away from discrete checkpoints, and towards a continuous manner. This change allows for the determination of exact failure times. Additionally, with the developed tool, the reduction of variability is seen in the Bell Test for when the operator is not around. This further provides for a reduction in error with lower rated ESCR polyethylenes. This improvement is solely due to the proposed monitoring system being on par with the operator. With this proposed tool being compared to an singular operator, the standardization of failure can be achieved, allowing for series of convolutional neural networks to effectively determine failures at different company sites. In return, this allows for a better reporting of ESCR values along the entire polyethylene manufacturing industry.

Acknowledgements

The authors would like to thank Imperial Oil LTD. for their funding of this work. The authors would like to especially thank Ron Cooke at Imperial Oil for his advice, supply of materials, and technical discussions throughout the exploration of the stress cracking fluid-polyethylene boundary within the Bell-Test. We would further like to thank Heera Marway at the McMaster Manufacturing Research Institute (MMRI) for assisting with the initial recording set up of the Bell Test, and finally Hassan Abdulhussain and Austin Bedrosian at McMaster University for their helpful insights with the convolutional neural networks present in this study.

References

[1] T.E. Nowlin, Business and Technology of the Global Polyethylene Industry, 2014.

[2] S. Ronca, Polyethylene, Elsevier Ltd, 2017. https://doi.org/10.1016/B978-0-323-35824-8.00010-4.

[3] M. Demirors, The History of Polyethylene, 2011. https://doi.org/10.1007/978-1-4614-6504-1_1.

[4] L.M. Robeson, Environmental Stress Cracking: A Review, Polymer Engineering & Science. 53 (2013) 453–467. https://doi.org/10.1002/pen.

[5] R.P. Brown, Testing plastics for resistance to environmental stress cracking, Polymer Testing. 1 (1980) 267–282. https://doi.org/10.1016/0142-9418(80)90010-0.

[6] ASTM, ASTM D1693.21 - Standard Test Method for Environmental Stress-Cracking of Ethylene Plastics, ASTM International. (2021) 1–11. https://doi.org/10.1520/D1693-21.2.

[7] M. Drvoderic, M. Rettl, M. Pletz, C. Schuecker, CrackDect: Detecting crack densities in images of fiber-reinforced polymers, SoftwareX. 16 (2021) 100832. https://doi.org/10.1016/j.softx.2021.100832.

[8] S.Y. Wang, P.Z. Zhang, S.Y. Zhou, D.B. Wei, F. Ding, F.K. Li, A computer vision based machine learning approach for fatigue crack initiation sites recognition, Computational Materials Science. 171 (2020). https://doi.org/10.1016/j.commatsci.2019.109259.

[9] G. Wang, P.W. Tse, M. Yuan, Automatic internal crack detection from a sequence of infrared images with a triple-threshold Canny edge detector, Measurement Science and Technology. 29 (2018). https://doi.org/10.1088/1361-6501/aa9857.

[10] ASTM International, Standard Practice for Compression Molding Thermoplastic Materials into Test Specimens, Plaques, or Sheets, (2016) 1–13. https://doi.org/10.1520/D4703-16.2.

[11] J. Redmon, A. Farhadi, YOLO v.3, Tech Report. (2018) 1–6. https://pjreddie.com/media/files/papers/YOLOv3.pdf.

[12] A.W. Bowman, R.B. D'Agostino, M.A. Stephens, Goodness-of-Fit Techniques., Journal of the Royal Statistical Society. Series A (Statistics in Society). 151 (1988) 225. https://doi.org/10.2307/2982198.

Chapter 6. Conclusions and Future Work

This thesis focused on improving the understanding of environmental stress cracking of polyethylene's through modifications and improvements to the Bell Test. The exploration of improving the Bell Test led to the development of a novel notching technique based on the principles of annealing, a better understanding of how local crystalline morphology affects the environmental stress cracking mechanism, and finally an automated and standardized tool to evaluate specimens undergoing the Bell Test.

6.1 Key Findings and Contributions

Findings which arose from the research in this thesis are summarized below.

1. Increased reproducibility of failure times from heat notching was seen between the cold crystallization temperature and melting temperature due to a reduction in crystallinity, tie molecules, and interlamellar linkages. Heat notching was additionally very local to the notch and was thought to aid in IGEPAL CO-630 absorption into the semi crystalline structures beneath the amorphous surface area.
2. The higher crystallinity due to heat notching as seen through atomic force microscopy, contact angle measurement, and roughness measurements, provided for higher surface energies as well as smoother surfaces. With smoother surfaces and higher surface energies present at the notch, an increased opportunity for IGEPAL CO-630 to diffuse into the notched surface quicker then the original notching method was present.
3. Bromocresol Green proved to be a novel visualization tool for tracking how IGEPAL CO-630 absorbed into polyethylene specimens. Bromocresol Green was

noted to incorporate itself into IGEPAL CO-630's micelles, and by its presence allowed for surfactant absorption to be directly monitored as the stress concentrated notch expanded in polyethylene specimens.

4. Simultaneous analysis of IGEPAL CO-630's absorption, stress development, and notch expansion, and their interactions of each overtime led to a better understanding on how polyethylene fails by the Bell Test. Using these three metrics as well as their relationship led to the development of the *plasticization threshold*, where crystallinity as well as tie molecules can delay as well as accelerate the point at which the specimen faces the *plasticization threshold*. After the *plasticization threshold* is achieved, IGEPAL CO-630 accelerates stresses as well as notch dilation for failure to occur.
5. In both the heat notching technique as well as the exploration of absorption, stress development, and notch expansion, local crystalline morphology can dictate how environmental stress cracking may delay or accelerate failure.
6. Automation of the Bell Test by a series of convolutional neural networks was shown to reduce the variability of failure times noted in the Bell Test. This was done by moving the Bell test away from discrete checkpoints and towards a continuous manner.

6.2 Future Work

To further understand the environmental stress cracking mechanism in polyethylene, the bulk properties of the Bell Test strips should be modified or altered during

the preparation process and compared to ASTM-D4703's process. Examples of altering the preparation process include, quenching, annealing, ramping up of temperature during the compression stage, and various compression pressures within the hot-press. Failure times of all these specimens as well as different grades of polyethylene should be recorded.

Once this data is collected, Transmission Electron Microscopy and Atomic Force Microscopy of failure sites as well as the notch should be conducted to understand how the crystalline structures failed and reacted to the Bell Test. With this information, a numerical model as well as a finite element model depicting randomized crystalline and amorphous orientations and structures can be developed. The model can be used to first predict how these conditions will affect the time of failure, and secondly predict how various preparation methods affect the crystalline and amorphous structures and their reaction to the Bell Test. With both the numerical model and finite element model predicting when failure will occur as well as how the crystalline and amorphous structures fail accordingly to their conditions, the computer vision model produced in this thesis can be used to validate the results of both models through failure time.

The functioning computer vision model automating and standardizing the Bell Test in this thesis, can provide industry with a standardized reporting of ESCR ratings for polyethylene. It is believed that this computer vision model may help industry rapidly determine ideal processing conditions of polyethylene products that are exposed to various chemicals. With a faster determination of ideal processing conditions of polyethylene parts, increased monetary savings in both material and labour will occur. A white paper based on

this computer vision model should be produced and marketed to downstream polyethylene users.